Molecular Recognition at Organic-Inorganic Interface in Biomineralization Processes

Giuseppe Falini – Simona Fermani

Biomineralization and Biocrystallography Group
Dipartimento di Chimica “Giacomo Ciamician”

Biomineralization: the processes by which organisms form minerals

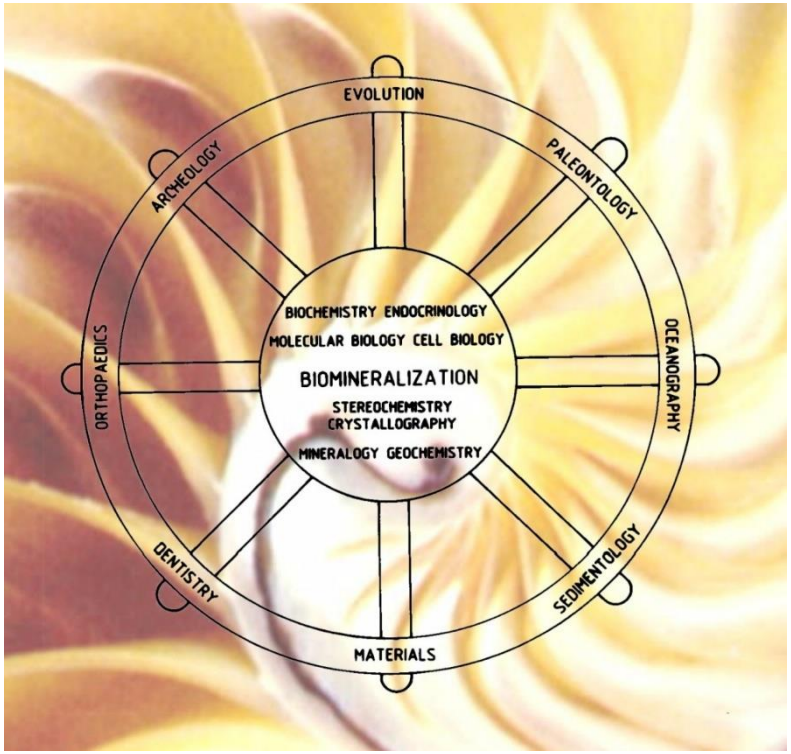

"Biomineralization links soft organic tissues, which are compositionally akin to the atmosphere and oceans, with the hard materials of the solid Earth. It provides organisms with skeletons and shells while they are alive, and when they die these are deposited as sediment in environments from river plains to the deep ocean floor. It is also these hard, resistant products of life which are mainly responsible for the Earth's fossil record. Consequently, biomineralization involves biologists, chemists, and geologists in interdisciplinary studies at one of the interfaces between Earth and life."
(Leadbeater and Riding 1986)

Over the last 3500 Myr or so, first prokaryotes and then eukaryotes developed the ability to form minerals. From that time organisms from many different phyla evolved the ability to form the almost 76 different minerals known to date.

Name	*Formula*
Carbonates	
Calcite	$CaCO_3$
Mg-calcite	$(Mg_xCa_{1-x})CO_3$
Aragonite	$CaCO_3$
Vaterite	$CaCO_3$
Monohydrocalcite	$CaCO_3 \cdot H_2O$
Protodolomite	$CaMg(CO_3)_2$
Hydrocerussite	$Pb_3(CO_3)_2(OH)_2$
Amorphous Calcium Carbonate (at least 5 forms)	$CaCO_3 \cdot H_2O$ or $CaCO_3$
Phosphates	
Octacalcium phosphate	$Ca_8H_2(PO_4)_6$
Brushite	$CaHPO_4 \cdot 2H_2O$
Francolite	$Ca_{10}(PO_4)_6F_2$
Carbonated-hydroxylapatite (dahllite)	$Ca_5(PO_4,CO_3)_3(OH)$
Whitlockite	$Ca_{18}H_2(Mg,Fe)_2^{+2}(PO_4)_{14}$
Struvite	$Mg(NH_4)(PO_4) \cdot 6H_2O$
Vivianite	$Fe_3^{+2}(PO_4)_2 \cdot 8H_20$
Amorphous Calcium Phosphate (at least 6 forms)	variable
Amorphous Calcium Pyrophosphate	$Ca_2P_2O_7 \cdot 2H_2O$
Sulfates	
Gypsum	$CaSO_4 \cdot 2H_2O$
Barite	$BaSO_4$
Celestite	$SrSO_4$

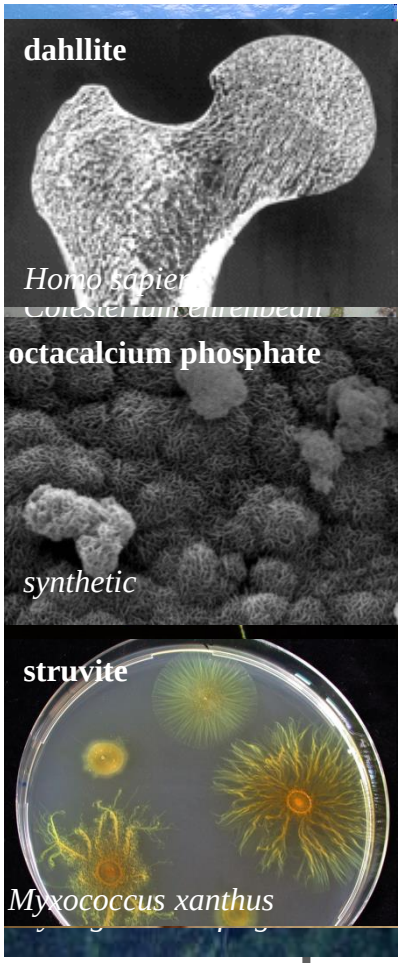

Over the last 3500 Myr or so, first prokaryotes and then eukaryotes developed the ability to form minerals. From that time organisms from many different phyla evolved the ability to form the almost 76 different minerals known to date.

Name	*Formula*
Oxides	
Magnetite	Fe_3O_4
Amorphous Ilmenite	$Fe^{+2}TiO_3$
Amorphous Iron Oxide	Fe_2O_3
Amorphous Manganese Oxide	Mn_3O_4
Hydroxides & Hydrous Oxides	
Goethite	α-FeOOH
Lepidocrocite	γ-FeOOH
Ferrihydrite	$5Fe_2O_3 \cdot 9H_2O$
Sulfides	
Pyrite	FeS_2
Hydrotroilite	$FeS \cdot nH_2O$
Sphalerite	ZnS
Wurtzite	ZnS
Organic Crystals*	
Earlandite	$Ca_3(C_6H_5O_2)_2 \cdot 4H_2O$
Whewellite	$CaC_2O_4 \cdot H_2O$
Weddelite	$CaC_2O_4 \cdot (2+X)H_2O$ (X<0.5)
Glushinskite	$MgC_2O_4 \cdot 4H_2O$
Arsenates	
Orpiment	As_2S_3
Hydrated Silica	
Amorphous Silica	$SiO_2 \cdot nH_2O$

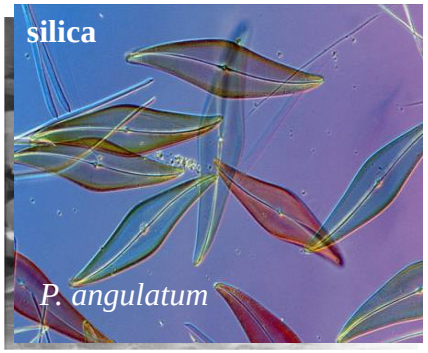

Biogenic Minerals or Biominerals

The term biomineral refers not only to a biogenic mineral, but also to the fact that these products are **composite materials** of both **mineral** and **organic components**.
Biomineral phases often have properties such as shape, morphology, size, crystallinity, isotopic and trace element compositions **quite unlike its inorganically formed counterpart**.
The term "**biomineral**" reflects all this complexity.

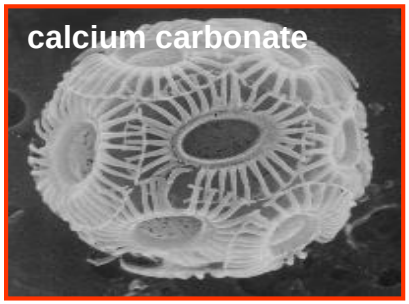

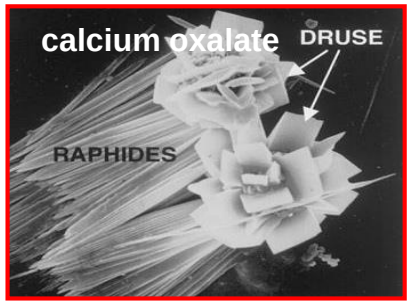

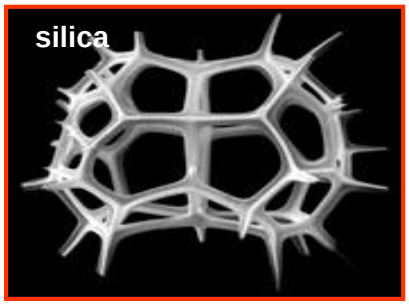

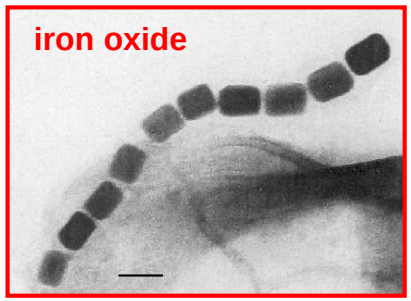

Organisms are able to control their mineralization at molecular level producing materials with an hierarchical organization ranging from the nano to the macro scale.

Biominerals: morphologies

Biominerals meet all the criteria for being true minerals.
Biogenic minerals have unusual external morphologies. The images of calcite single crystals below illustrate the astonishing ability of Nature to grow minerals of a complexity that is (for now) an impossible task for humankind to replicate!

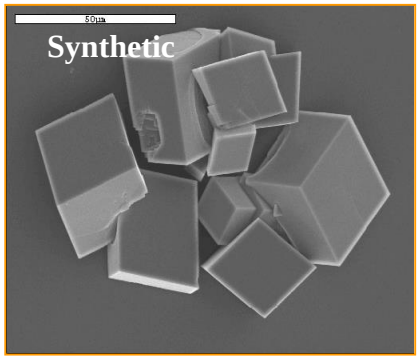

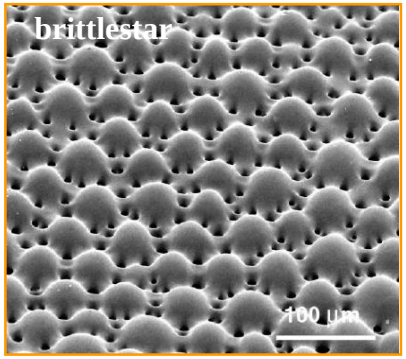

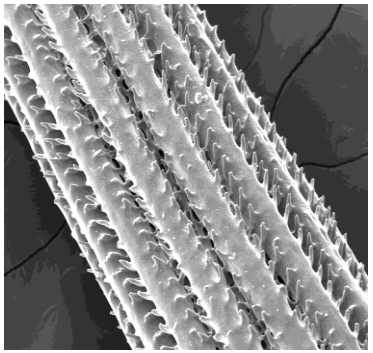

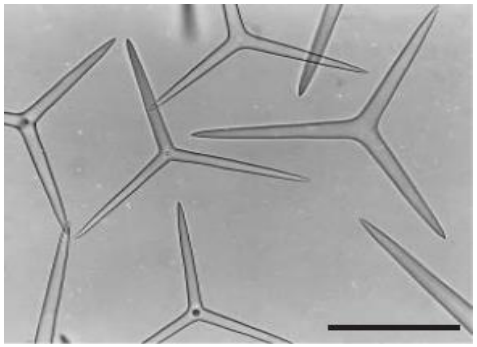

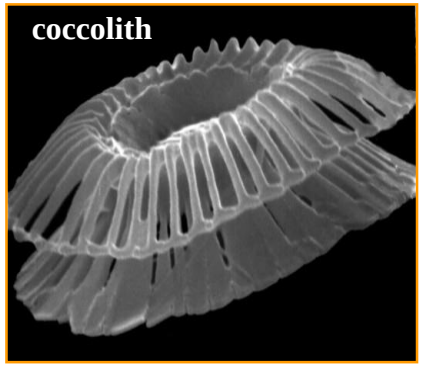

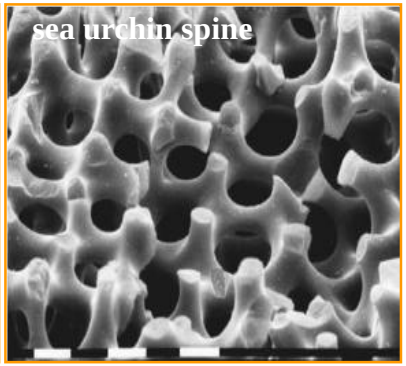

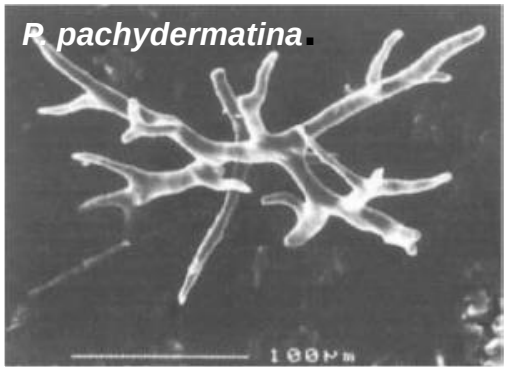

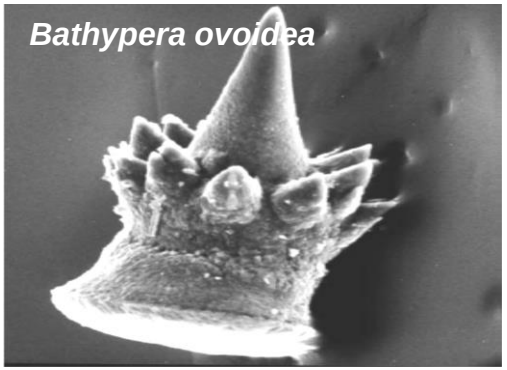

Genetic regulation runs the controlled-mineralization “program” to form biominerals with unusual morphologies using great fidelity again and again.

Biominerals: distribution

Organisms are able to deposit uncommon minerals and have a total control over their distribution.
This is genetically controlled and is almost always achieved with 100% fidelity.

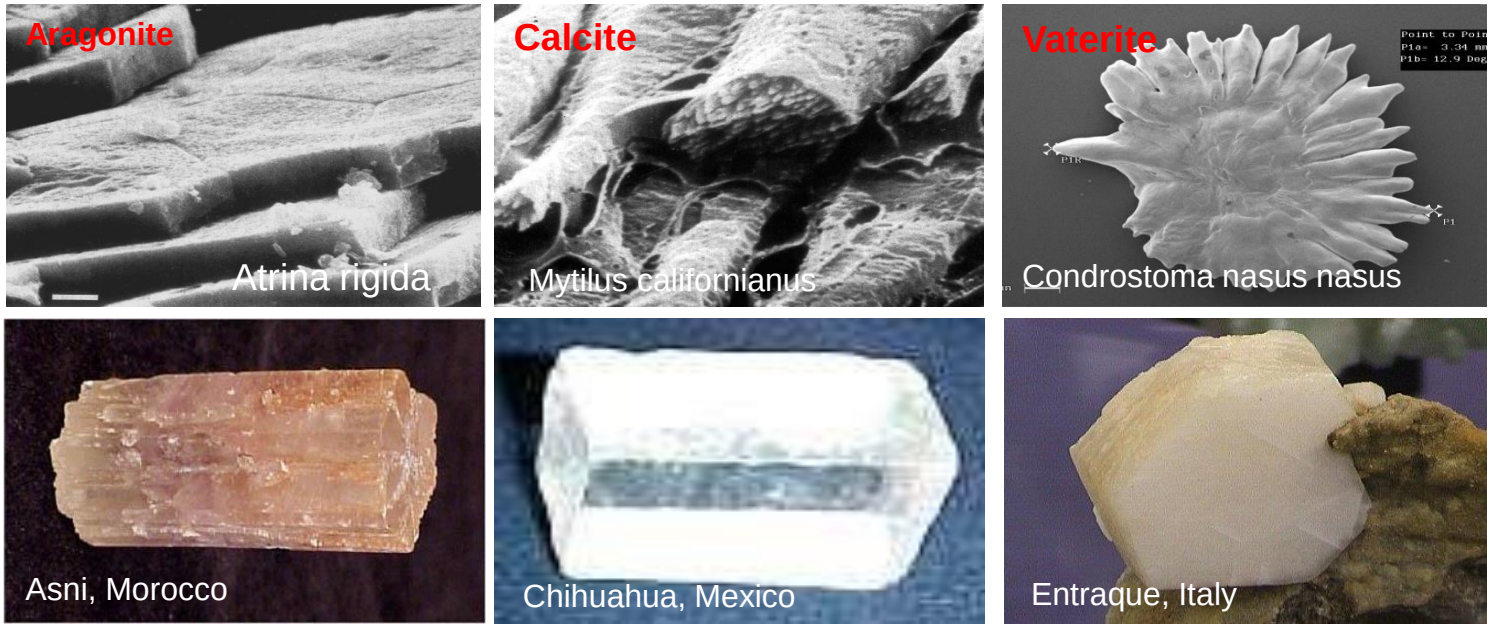

Biologically and abiologically produced anhydrous $CaCO_3$ mineral phases

Biominerals: polymorphic control

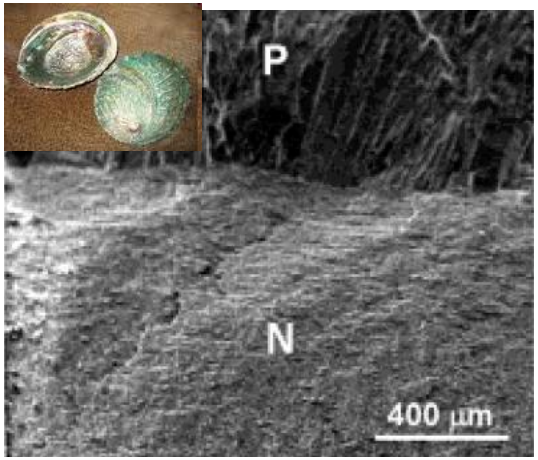

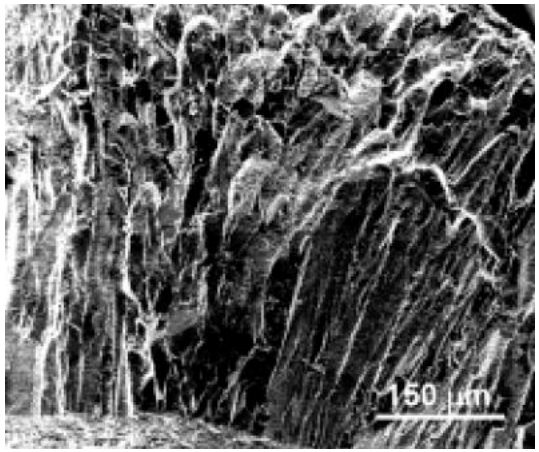

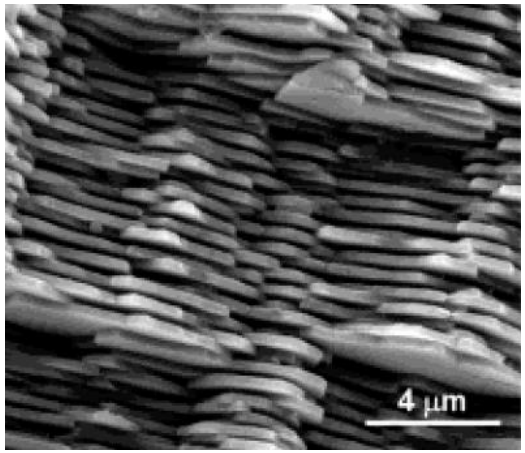

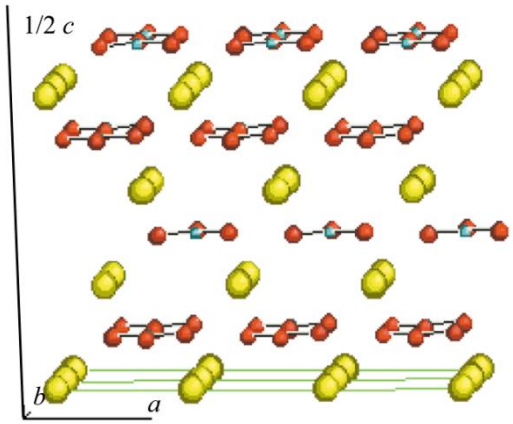

calcite

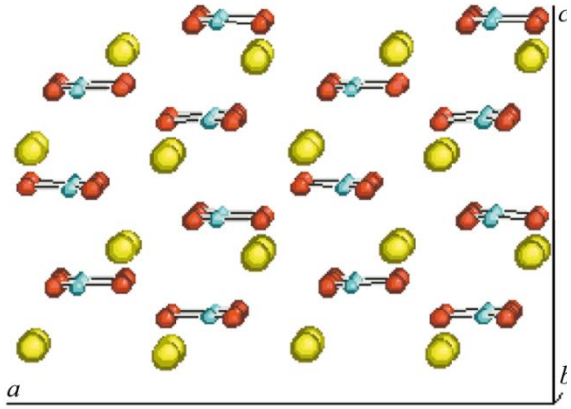

aragonite

Biominerals: mechanical properties

Biominerals such as bone, tooth, and nacre are nanocomposites of macromolecules and minerals with superior strength

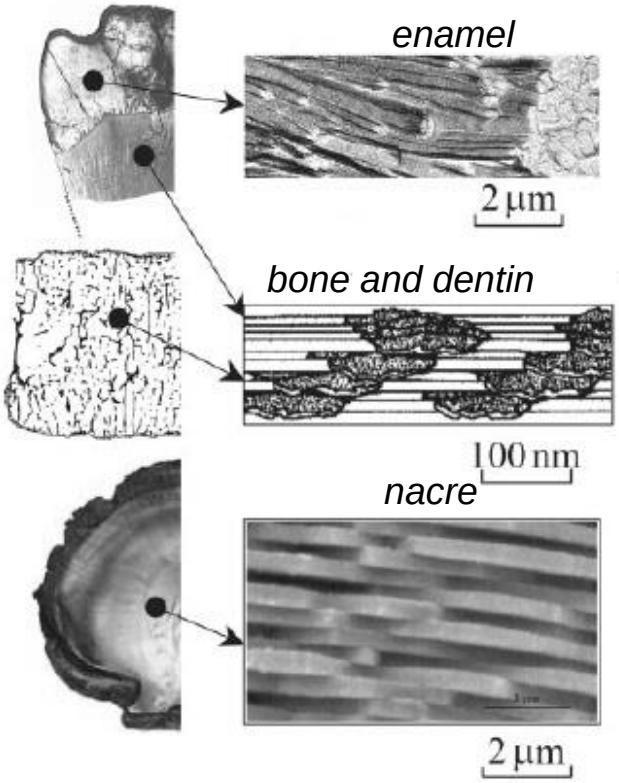

15-
1 (

2
1

250-500 nm thick
1-2 μm long

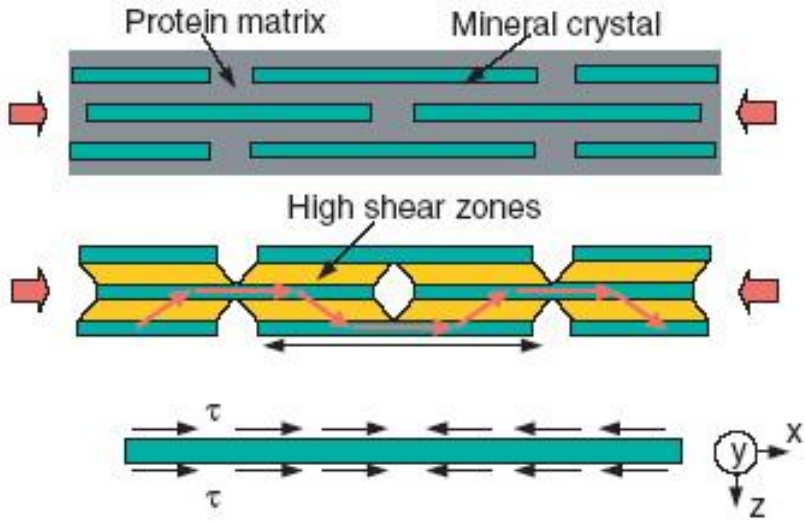

optimum strength and maximum robustness.

A model of biocomposites. A schematic diagram of staggered mineral crystals embedded in protein matrix. A simplified model showing the load-carrying structure of the mineral–protein composites. Most of the load is carried by the mineral platelets whereas the protein transfers load via the high shear zones between mineral platelets.

Many hard biological tissues, such as tooth, vertebral bone, or shells are made of hard mineral platelets in a soft (protein) matrix.

Biominerals are agglomerations of nano-crystals separated by **an organic matrix**. This can inter and/or intra crystalline and is **unique responsible** of the control over the mineral deposition.

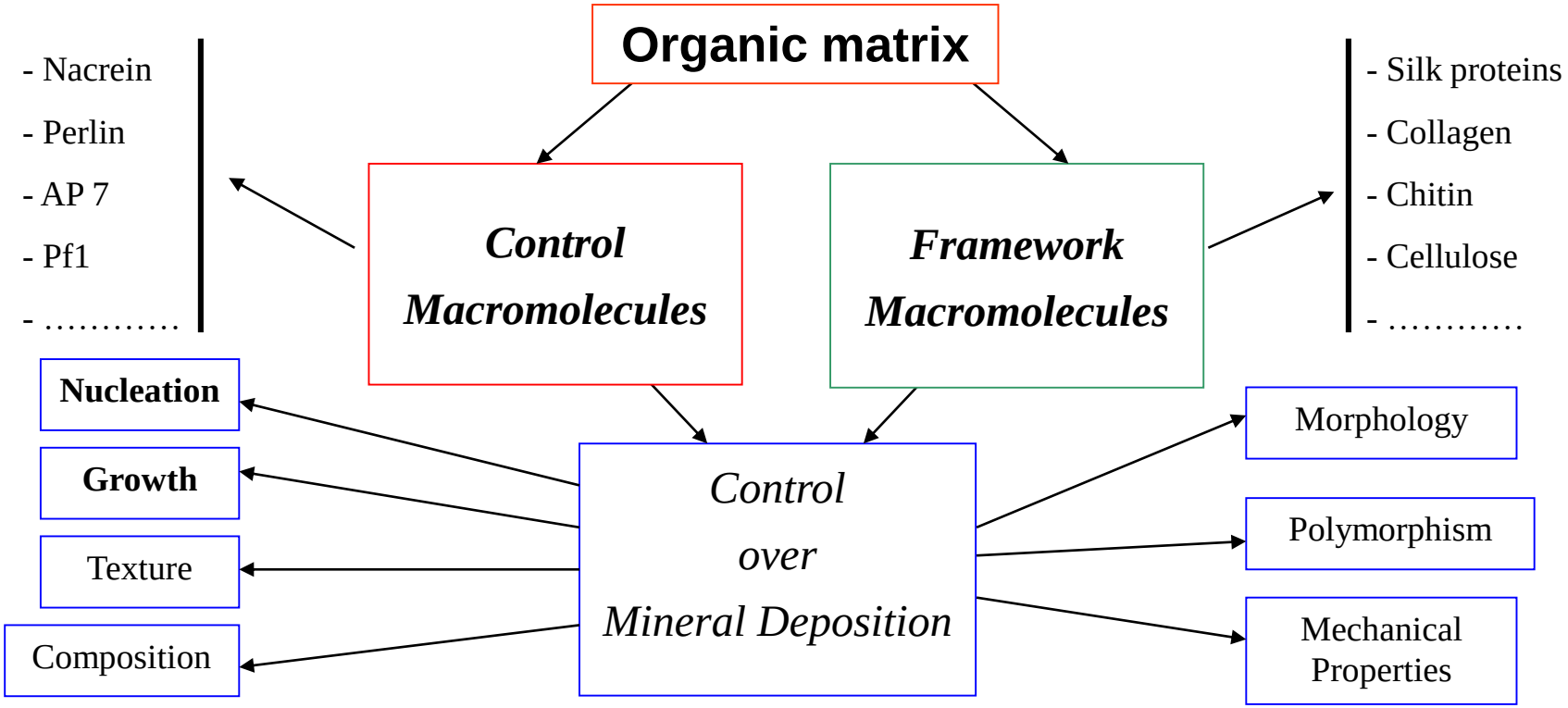

*The **spatial and temporal organization** of the organic matrix components are orchestrate at **cellular level**.*
This discriminates the degree of control over mineral deposition

Abalone shell: the Green Layer

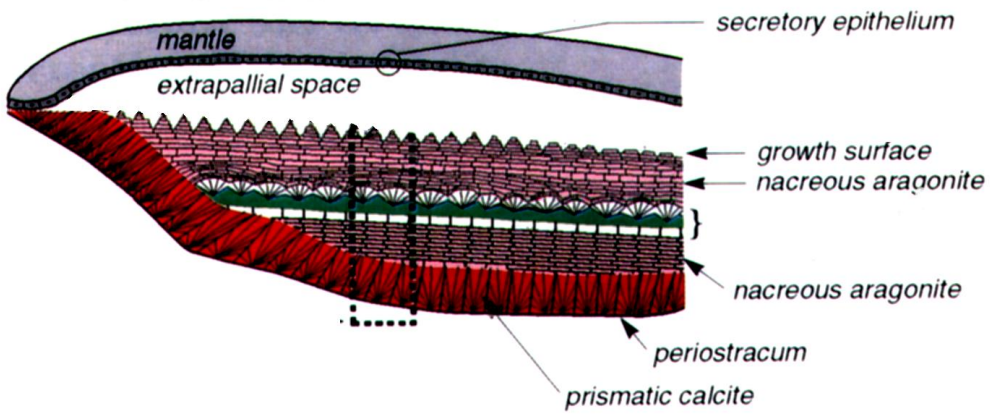

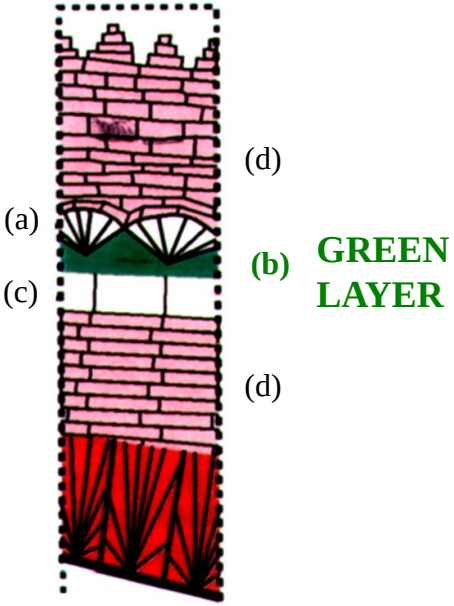

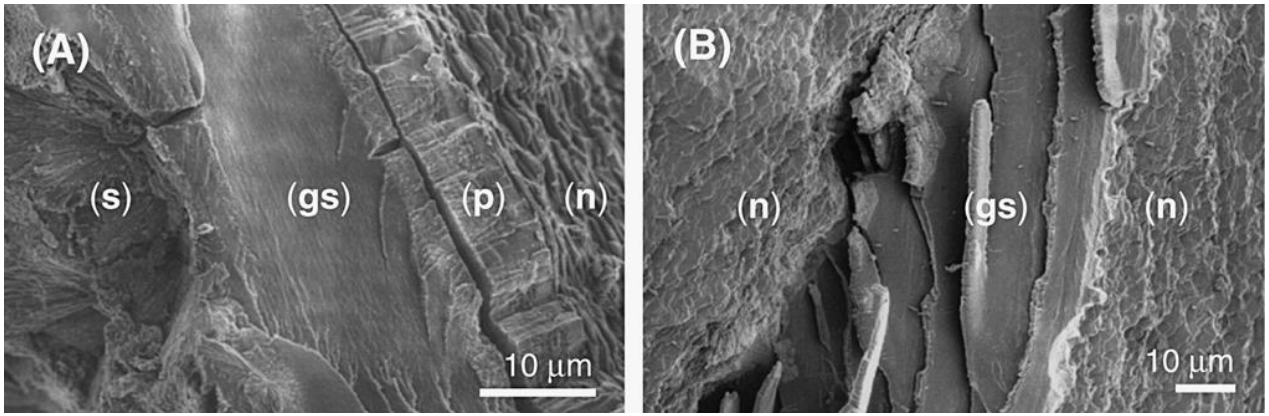

Scanning electron micrographs of a fragment of abalone shell nacre containing the green sheet.

Green Layer: Mineralogical Interface

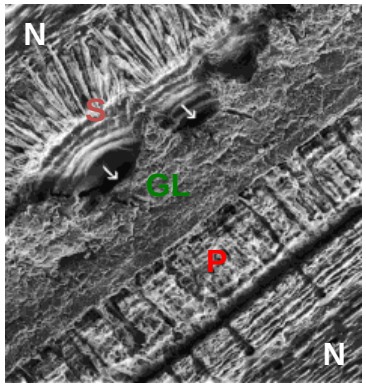

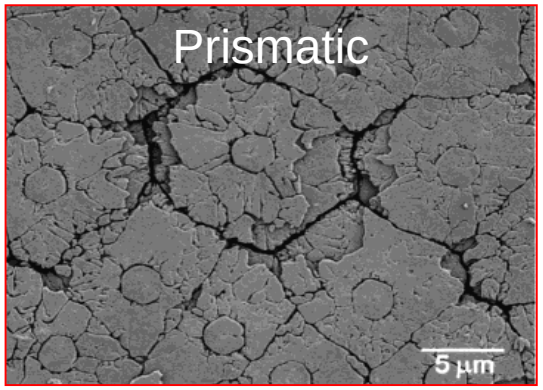

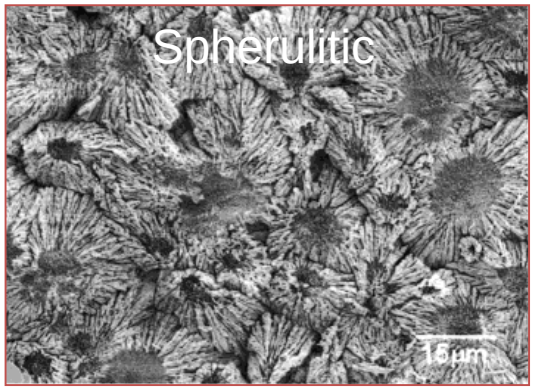

Cross-sectional SEM micgrograph showing a typical growth line in native red abalone shell.
Plan-view SEM micrograph of the prismatic and spherulitic microstructure.

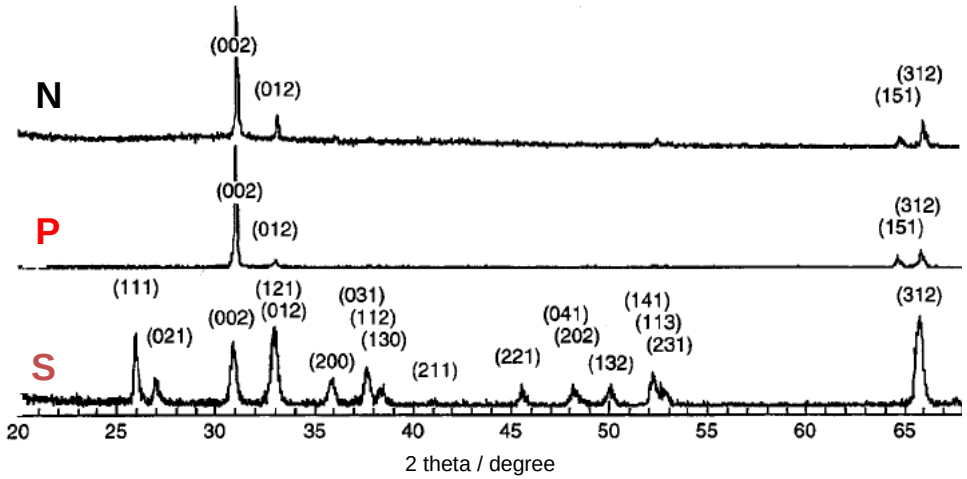

X-ray diffraction (XRD) pattern of the nacreous, prismatic, and spherulitic structures.

Green Layer: Morphological asymmetry

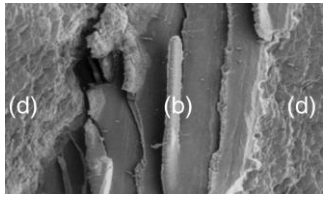

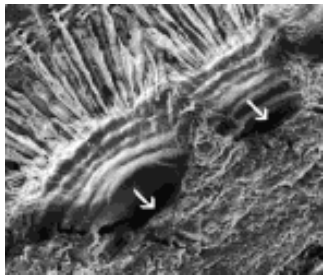

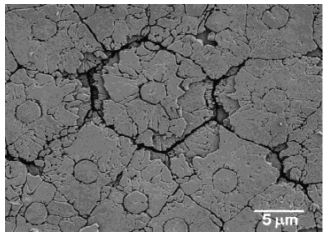

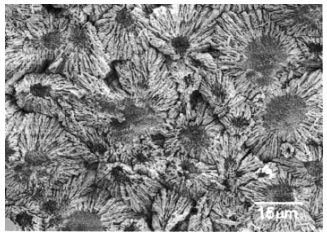

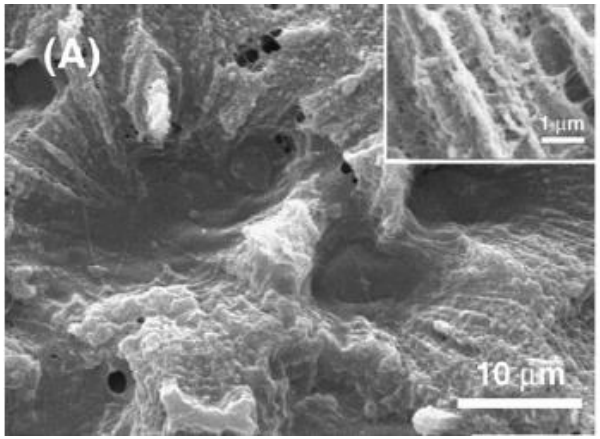

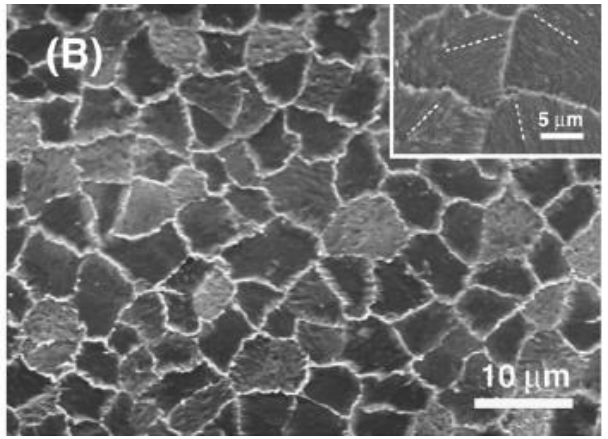

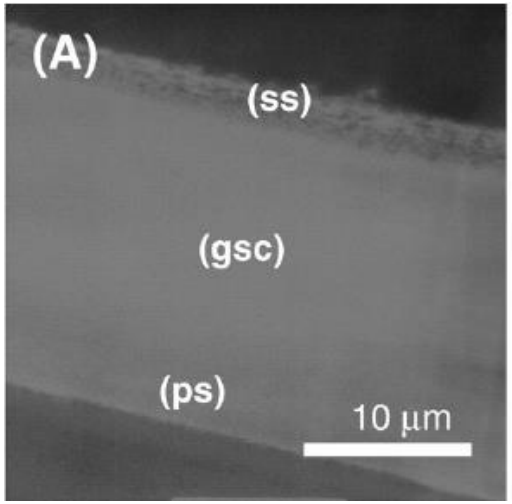

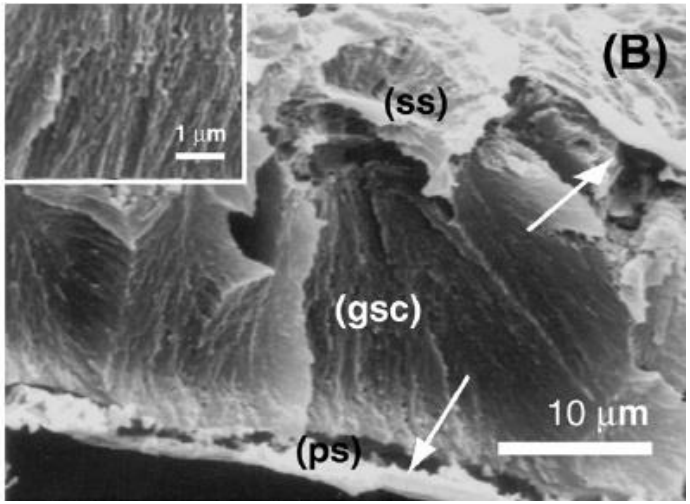

Scanning and transmission electron micrographs of the surfaces and cross section of the interstitial composite polymer sheet after demineralization. Up: (A**)** Surface facing spherulitic crystals. (B**)** Surface facing prismatic crystals

Green Layer: Compositional Asymmetry

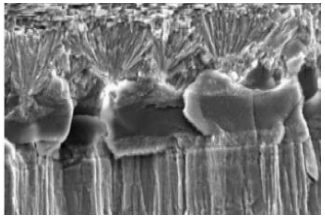

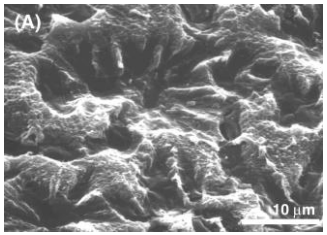

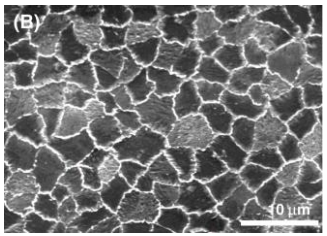

Table. Histochemical reactivities of the two surfaces of the interstitial polymeric composite sheet.

	Spherulitic Crystal-Facing Surface	Prismatic Crystal-Facing Surface
Coomassie blue	reactive	reactive
Schiff reagent	reactive	not reactive
DOPA assay	less reactive	more reactive
Cationic Carbocyanin	more reactive	less reactive

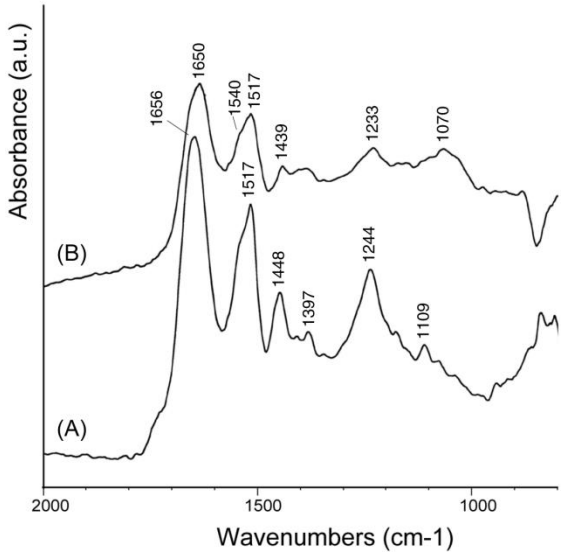

The faces of the green layer differ in their relative content of poly-saccharides and proteins

Green Layer: Fluorescence Asymmetry

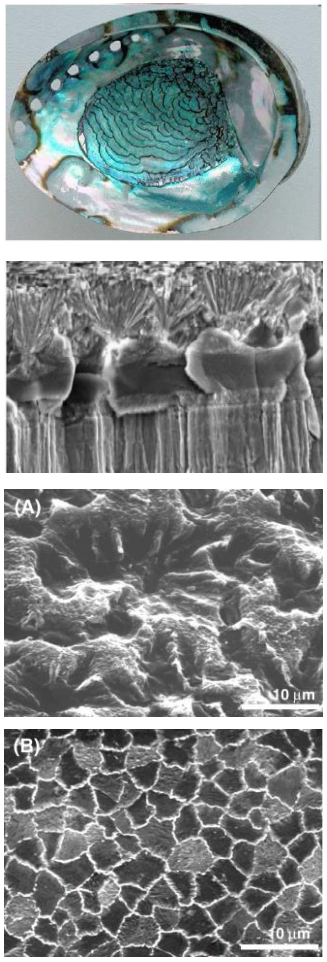

Fluorescence confocal microscopy

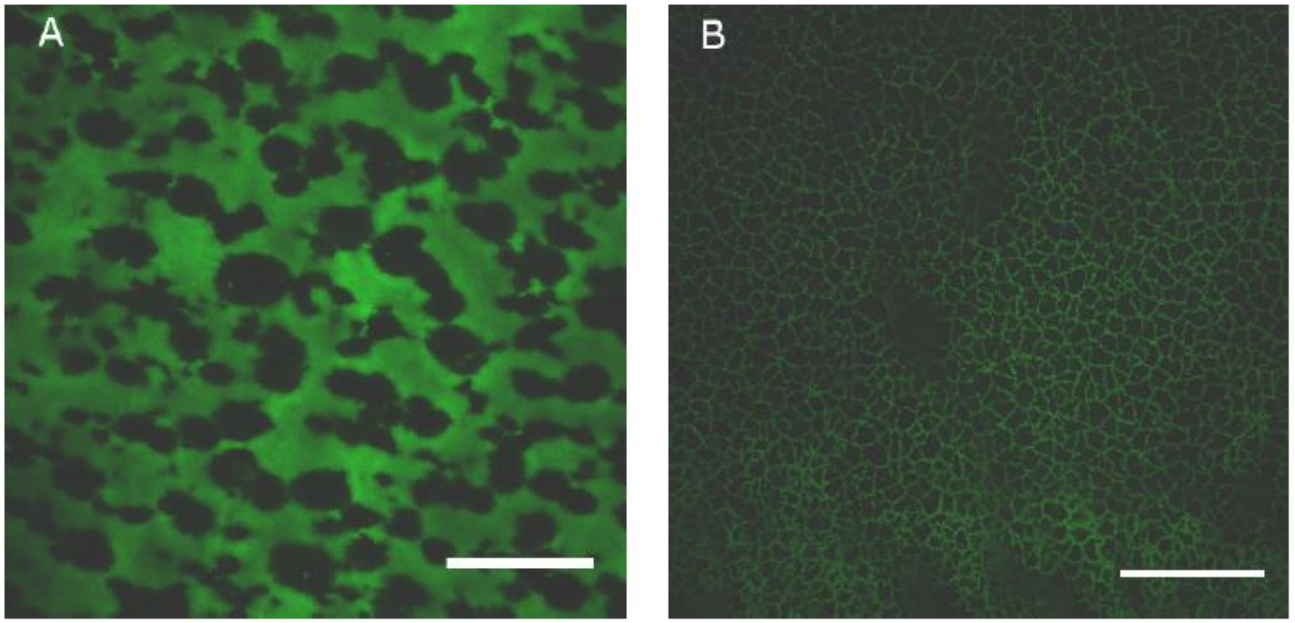

Confocal fluorescence micrographs exciting at 448 nm emission filter set at 520 nm bandpass. (A**)** Surface facing spherulitic crystals. (B**)** Surface facing prismatic crystals. Scale bar 50 µm.

Green Layer: Fluorescence Asymmetry

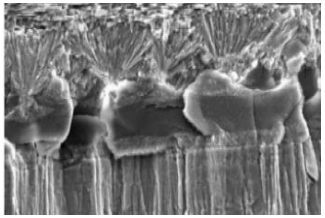

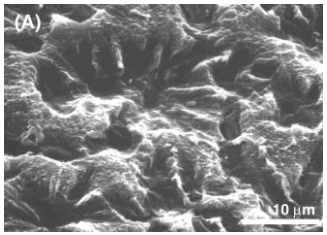

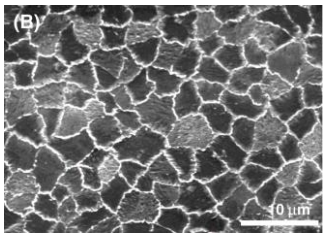

Fluorescence confocal microscopy

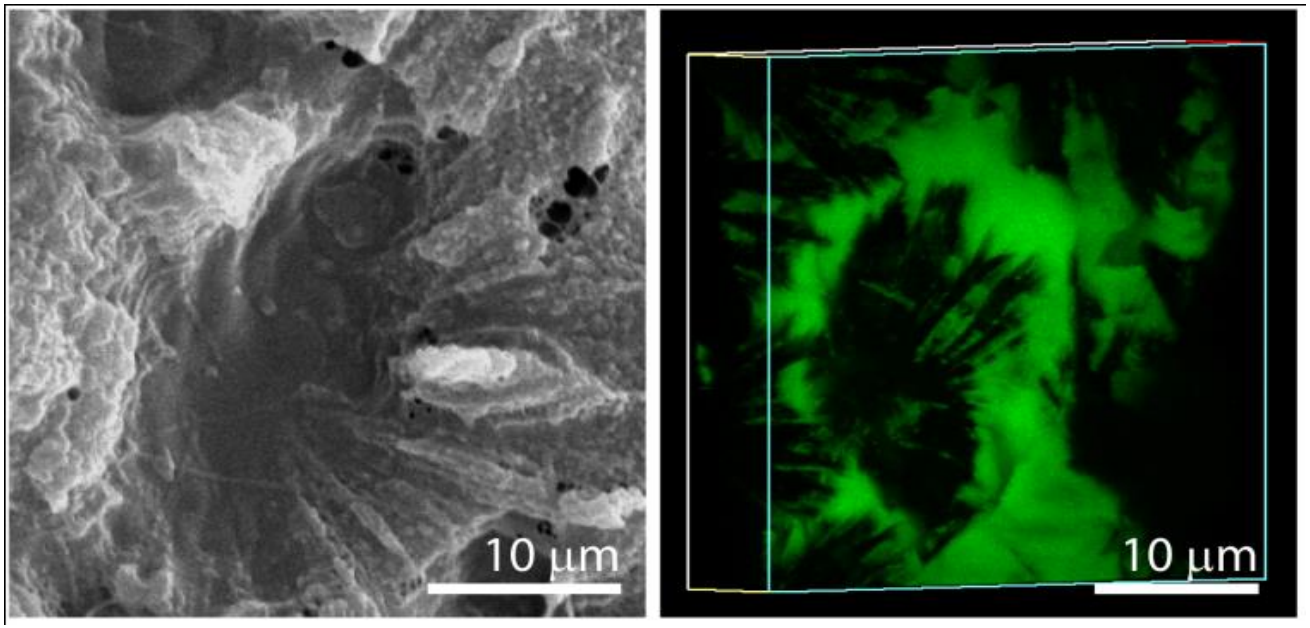

(left) Scanning electron microscopy image of the surface facing spherulitic crystals of the green sheet sides. (right) 3D confocal microscopy image of a fragment of the native nacre abalone shell containing an interdispesed green sheet.

Green Layer: Composition

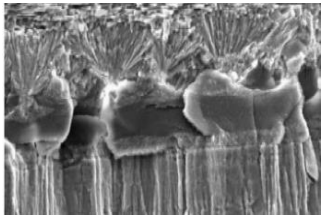

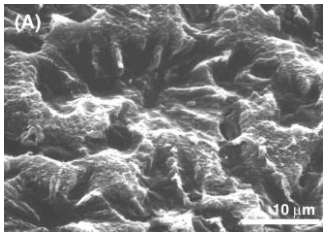

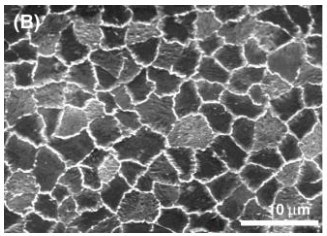

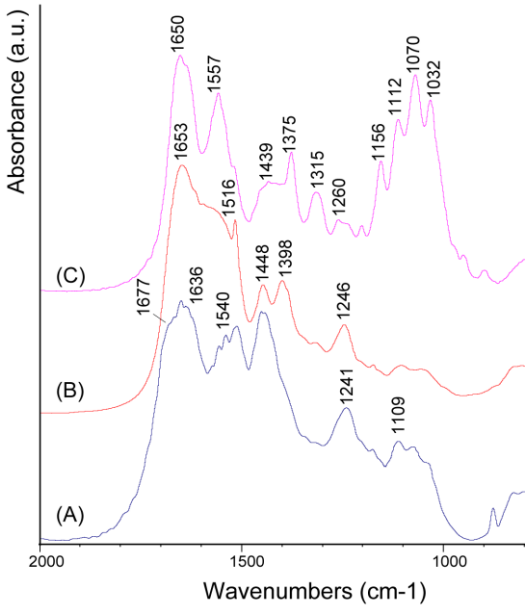

FTIR spectra. (A) Demineralized. (B) Soluble fraction and (C) insoluble fraction after extraction with 1 N NaOH of the interstitial polymer sheet

Table. 1. Amino acid and sugar composition of the interstitial polymer composite sheet (relative mol %). Polypeptide accounts for 60% of the material.

Amino Acids		Sugars	
Cys	1.0	Glucosamine	13.0
Asx	7.7	Glucose	13.0
MetSO2	0.1	Galactose	12.5
Thr	4.2	Mannose	3.9
Ser	6.0	Xylose	24.1
Glx	8.0	Arabinose	14
Pro	19.6	Other*	19.5
Gly	16.3		
Ala	1.7		
Val	4.4		
Ile	0.5		
Leu	1.5		
Tyr	17.6		
Phe	0.1		
His	4.4		
Lys	3.0		
Arg	3.9		

* This value refers to chromatographic peaks that could not be assigned.

Green Layer: Soluble macromolecules

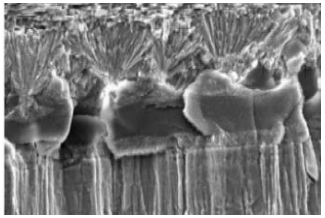

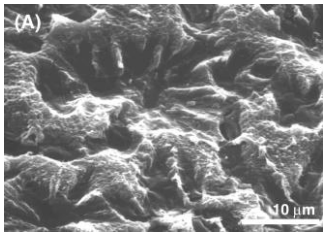

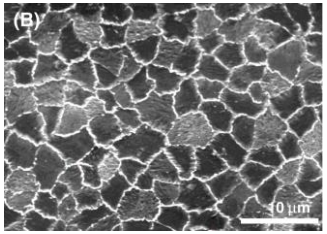

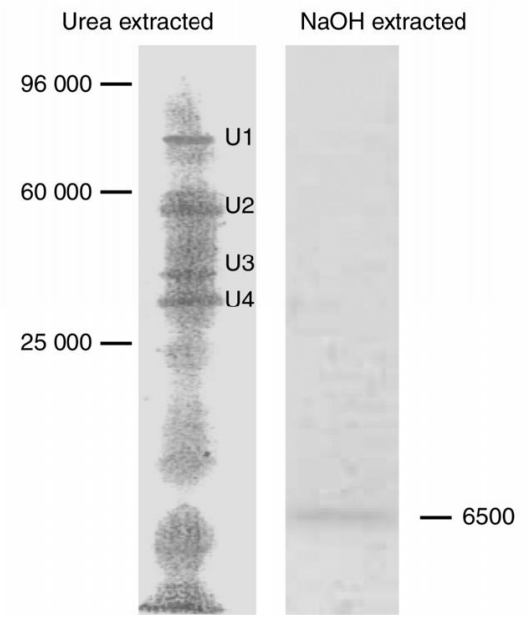

Table 2. Amino acid compositions (mol %) of protein fractions extracted from the interstitial polymeric composite sheet.

	U1	U2	U3	U4	NaOH-soluble
Cys	1.9	2.4	2.0	2.0	0.1
Asx	14.8	17.2	14.8	15.0	10.8
MetSO2	1.0		1.5	1.0	0.1
Thr	7.0	2.9	4.7	5.1	2.4
Ser	9.6	8.5	8.3	9.5	2.5
Glx	13.7	13.9	13.0	17.4	14.4
Pro	6.5	5.1	6.1	4.9	23.7
Gly	12.5	18.4	16.9	17.6	5.4
Ala	5.2	5.3	5.5	5.1	1.1
Val	5.2	3.8	4.6	4.2	7.3
Ile	3.3	2.7	3.7	3.3	0.8
Leu	5.8	5.4	5.5	5.8	2.2
Tyr	0.9	0.6	0.1	0.1	16.9
Phe	1.8	2.0	2.2	0.2	0.1
His	1.7	1.9	1.7	0.2	5.4
Lys	3.2	4.4	3.8	3.7	3.7
Arg	5.7	5.6	5.7	5.1	3.1

Solubilization obtained with 8 M urea, 3% (v/v) β-mercaptoethanol, 10 mM EDTA, 1% (w/v) SDS in sodium phosphate buffer (10 mM, pH 7.4). The solubilized proteins were resolved by electrophoresis on a 12% polyacrylamide gel under standard denaturing conditions and the gels stained with Coomassie Brilliant Blue R-250

Green Layer: nucleating properties

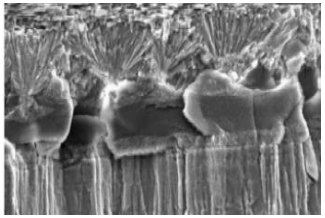

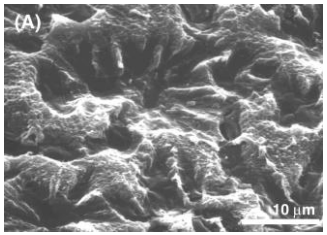

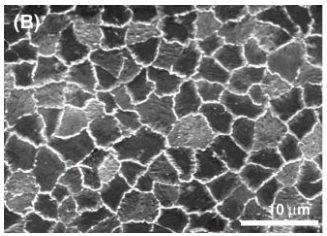

Table 3. Calcite crystals nucleating properties of the green layer.

	native form		carboxymethylated form	
	n° crystals*	crystal size**	n° crystals*	crystal size**
control***	37(18)	80(30)	41(23)	82(31)
g.l. s. side	33(14)	64(24)	25(10)	82(26)
g.l. p. side	101(34)	57(18)	27(10)	80(22)

* the number of crystals is referred to a surface area of 3 mm^2.
** Length (mm) along the main axis.
*** The control refers to the calcite crystals precipitated in the same conditions in the absence of green layer.

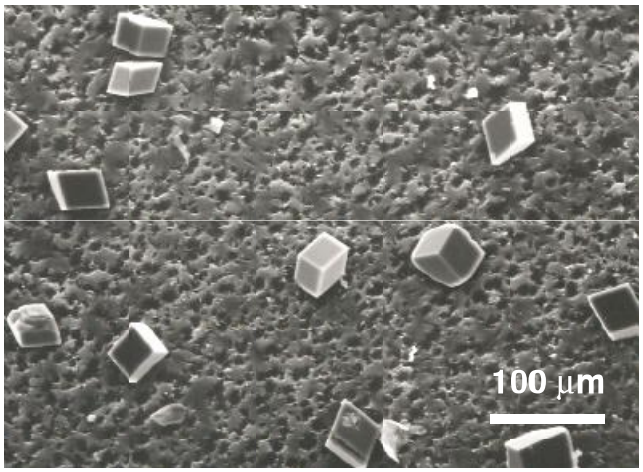

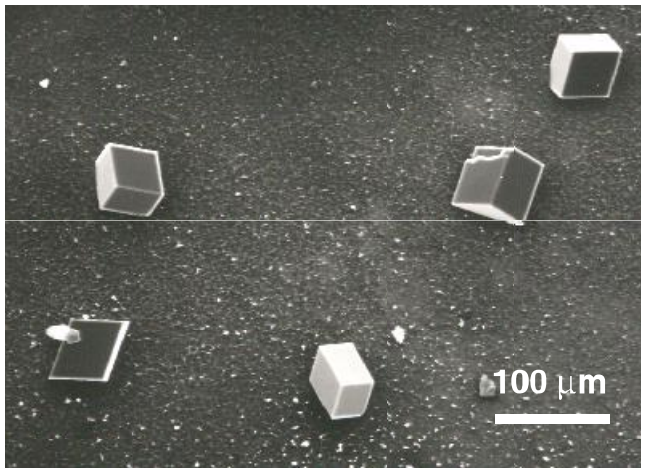

Green Layer: The alkaline extract.

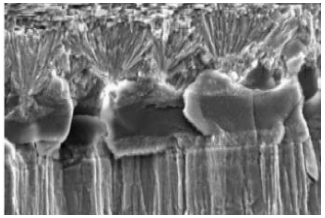

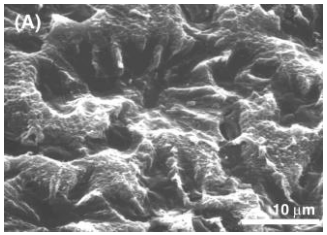

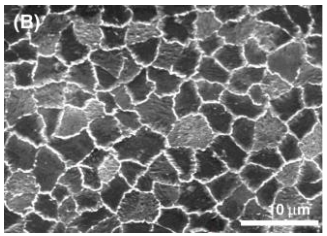

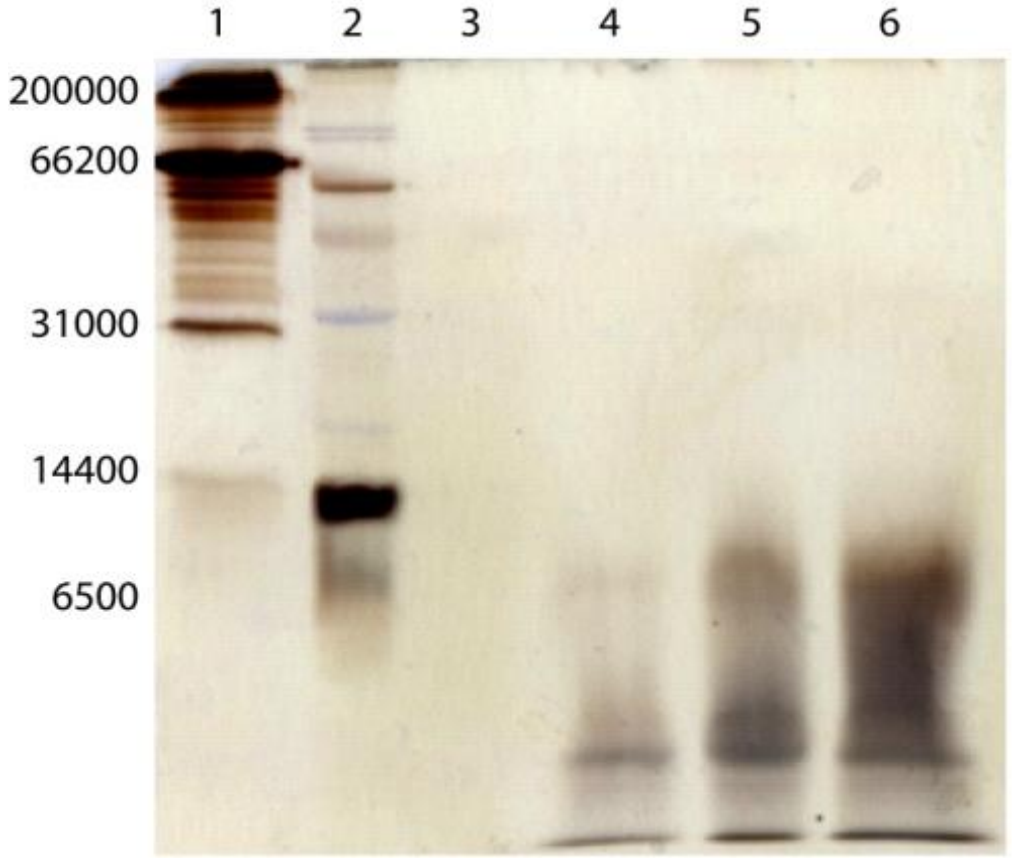

Cys	0.1
Asx	10.8
MetSO2	0.1
Thr	2.4
Ser	2.5
Glx	14.4
Pro	23.7
Gly	5.4
Ala	1.1
Val	7.3
Ile	0.8
Leu	2.2
Tyr	16.4
Phe	0.1
His	5.4
Lys	3.7
Arg	3.1

left. SDS-PAGE of GP solution conducted loading 30, 60 and 90 mg/ml in the lanes 4, 5 and 6, respectively. Lane 1 bovine serum albumin, lane 2 markers of different molecular weight, lane 3 empty. *right.* Amino acid compositions (mol%) of GP.

Green Layer: The alkaline extract.

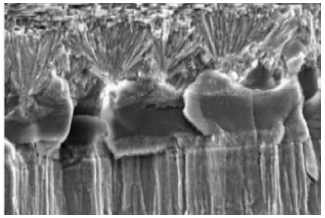

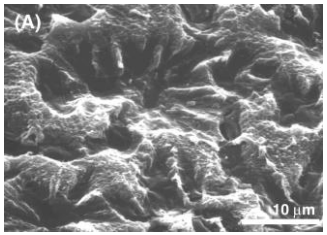

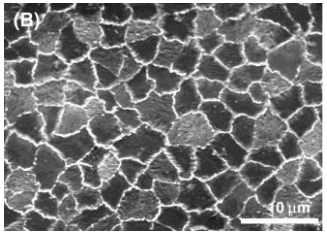

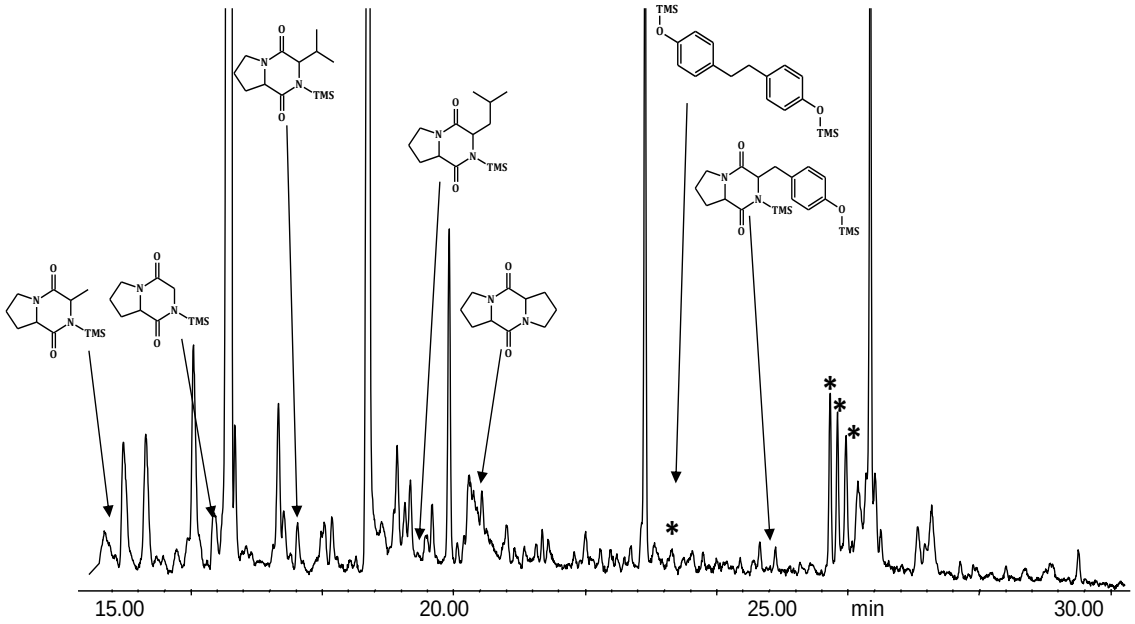

Cys	0.1
Asx	10.8
MetSO2	0.1
Thr	2.4
Ser	2.5
Glx	14.4
Pro	23.7
Gly	5.4
Ala	1.1
Val	7.3
Ile	0.8
Leu	2.2
Tyr	16.4
Phe	0.1
His	5.4
Lys	3.7
Arg	3.1

left. TIC GC-MS trace in the elution region of cyclodipeptides obtained from pyrolysis of GP after timethylsilylation. Starred peaks: silylated methyl phenol derivatives identified in the pyrolysate of dityrosine.*right.* Amino acid compositions (mol%) of GP.

Green Layer: The alkaline extract.

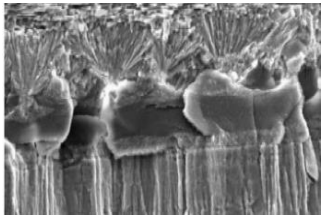

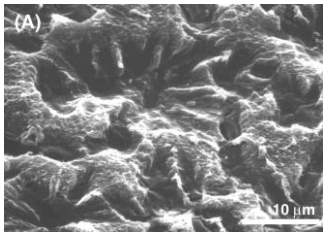

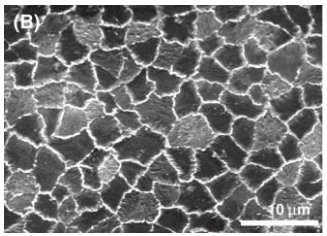

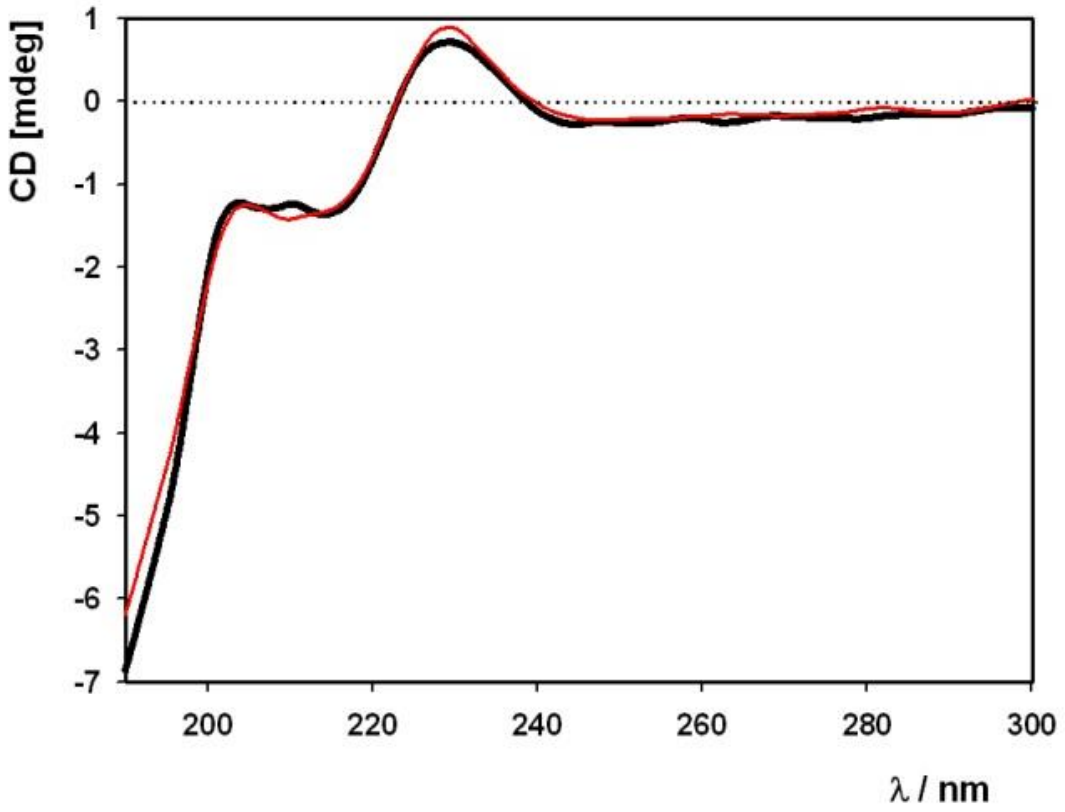

Cys	0.1
Asx	10.8
MetSO2	0.1
Thr	2.4
Ser	2.5
Glx	14.4
Pro	23.7
Gly	5.4
Ala	1.1
Val	7.3
Ile	0.8
Leu	2.2
Tyr	16.4
Phe	0.1
His	5.4
Lys	3.7
Arg	3.1

left. Far-UV CD spectra of GP in water solution (black line) and in a 0.25 mM solution of $CaCl_2$ in water (red line). *right.* Amino acid compositions (mol%) of GP.

Green Layer: The alkaline extract.

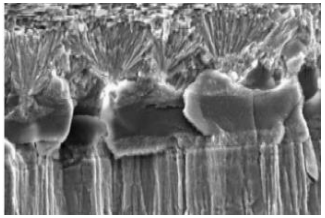

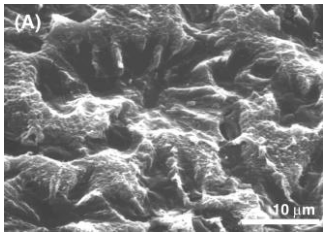

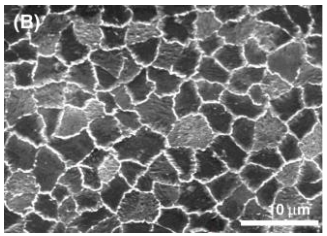

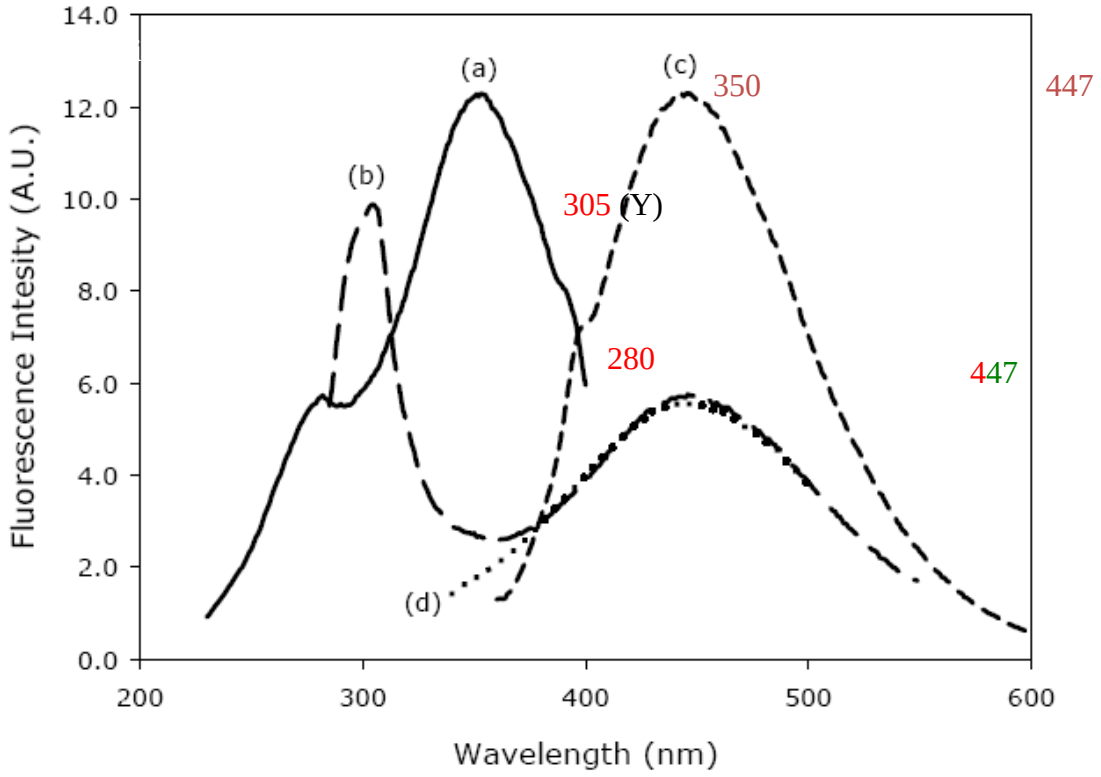

The fluorescence spectra shows a typical excitation band of aromatic aminoacid at 280 nm together with a more intense excitation band at 350 nm **(**a**)**; Emission spectrum with excitation wavelength at 280 nm **(**b**)**; at 350 nm **(**c**)**; and at 295 nm **(**d**)**.

Green Layer: The alkaline extract.

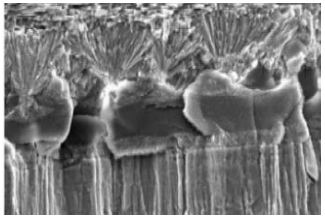

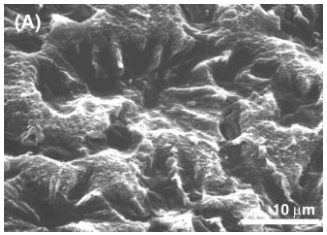

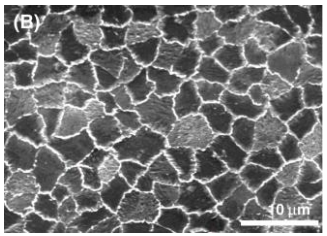

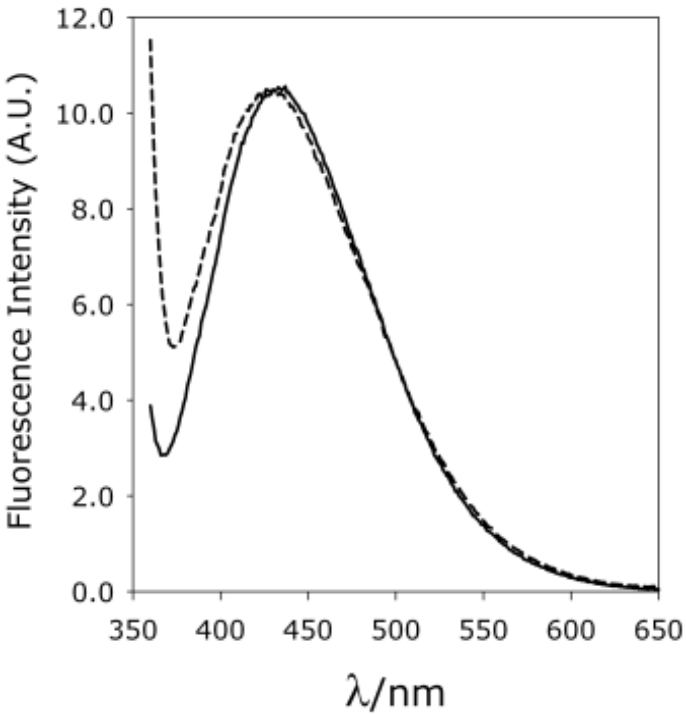

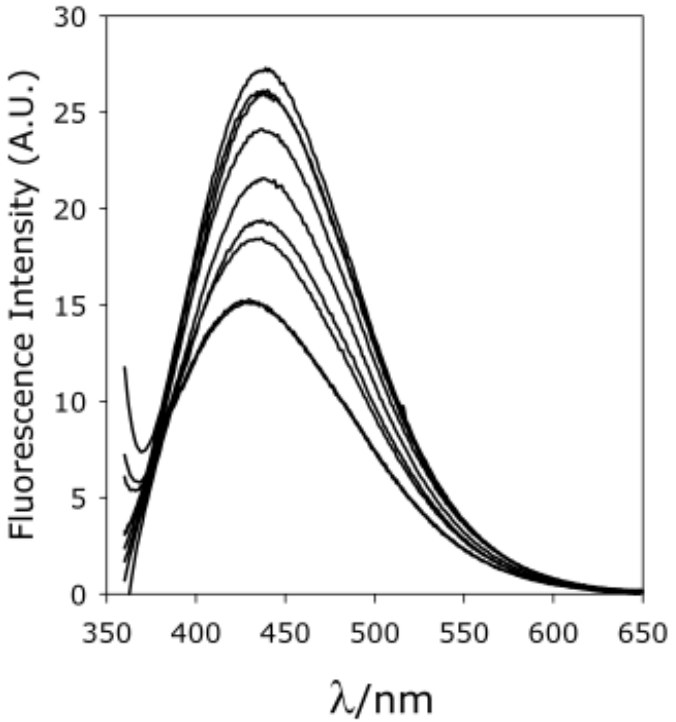

Fluorescence spectra of GP in water (dashed line) and in 10 mM $CaCl_2$ (solid line) upon excitation at 350 nm. (b) Fluorescence emission spectra of GP as a function of pH with 350 nm excitation. The increasing values of pH used were: 2.86, 3.57, 4.46, 5.04, 6.17, 6.62, 8.29, 9.19 and 9.90.

Green Layer peptide: $CaCO_3$ fluorescence

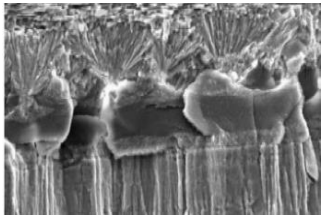

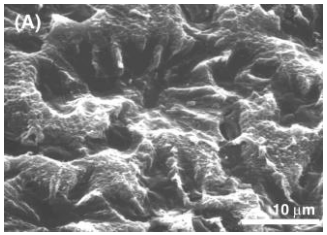

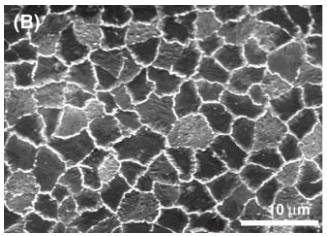

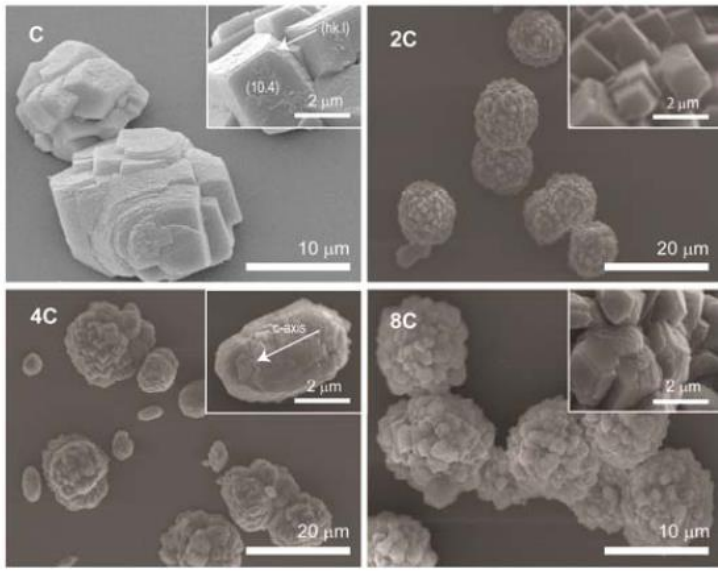

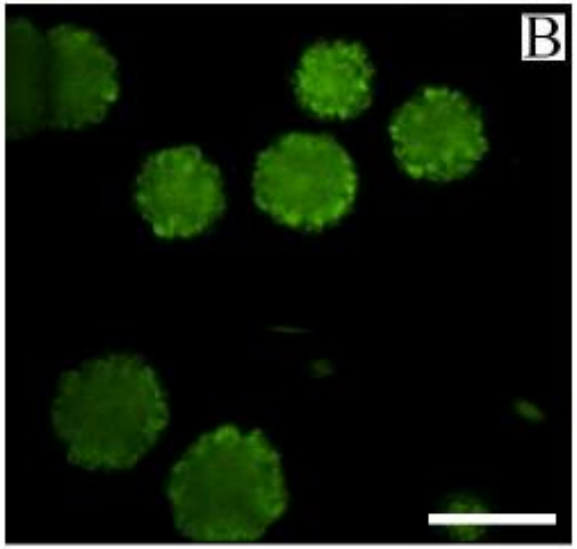

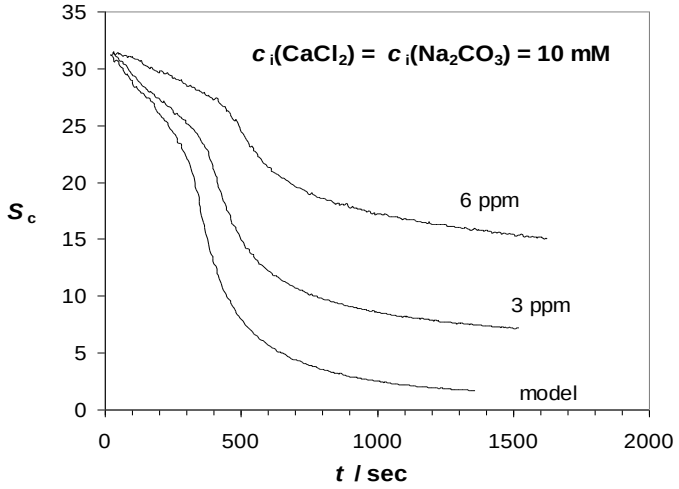

Progress curves, supersaturation versus time, of the spontaneous precipitation in the system of initial concentration of reactants, $c_i(Ca^{2+}) = c_i(CO_3^{2-}) = 0.010$ mol dm^{-3}, in the model system and in the systems containing different concentration of GP.

Green Layer peptide: $CaCO_3$ fluorescence

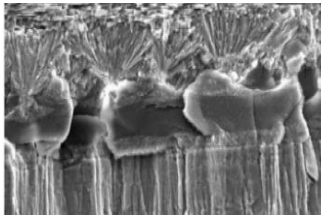

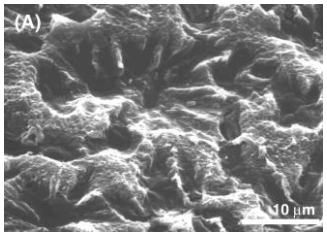

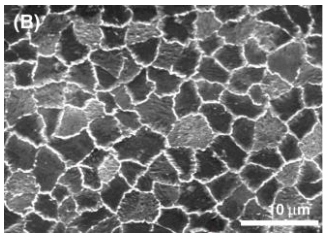

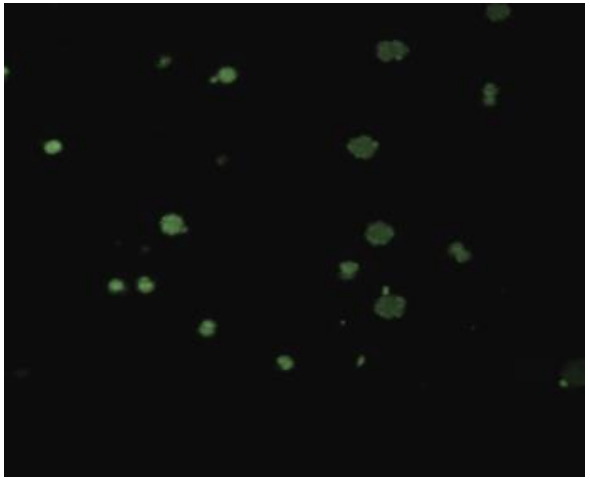

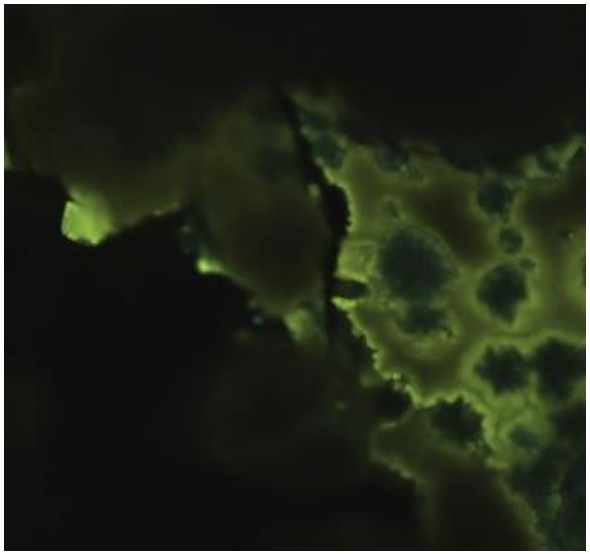

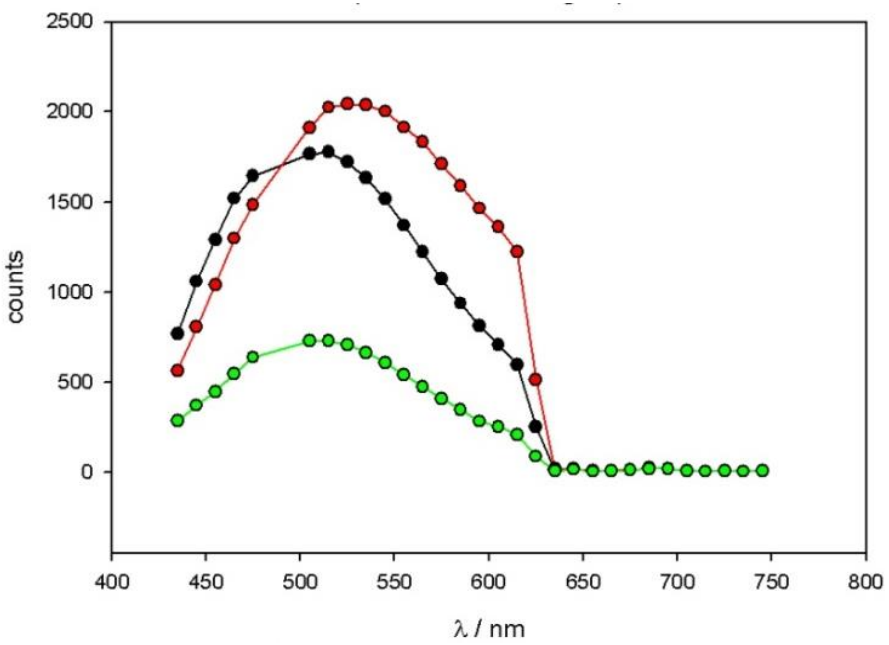

Confocal fluorescence spectroscopy images of calcite crystallized with GP the inner surface of a native abalone shell, in the vicinity of two green sheets.

Spectra of the peptide in solution (green), of the brightest fluorescent spots of crystals (black) and of the native shell (red).

Coral (bio)mineralization

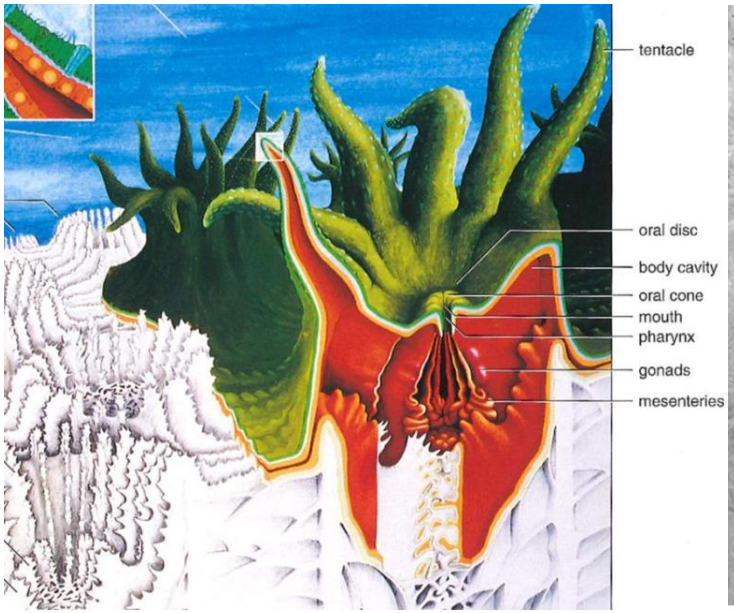

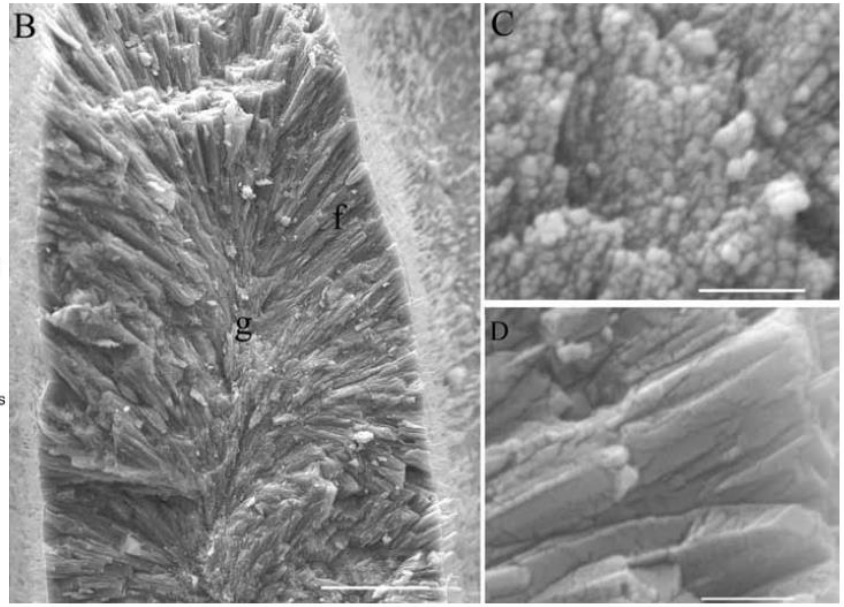

The coral animal (polyp) produce many millions of tiny calcium carbonate (aragonite) crystals that are assembled into a skeleton. In (A), each polyp in the colony builds its own skeleton, the corallite . The polyp sits atop of, and completely covers, the skeletal surface. In (B), the skeleton is composed of radiating arrays of needle-shaped crystals (D) that grow on aggregates of fine granular crystals (C). (*from Veron and Cohen*)

Coral skeletons – all sharing common feautures

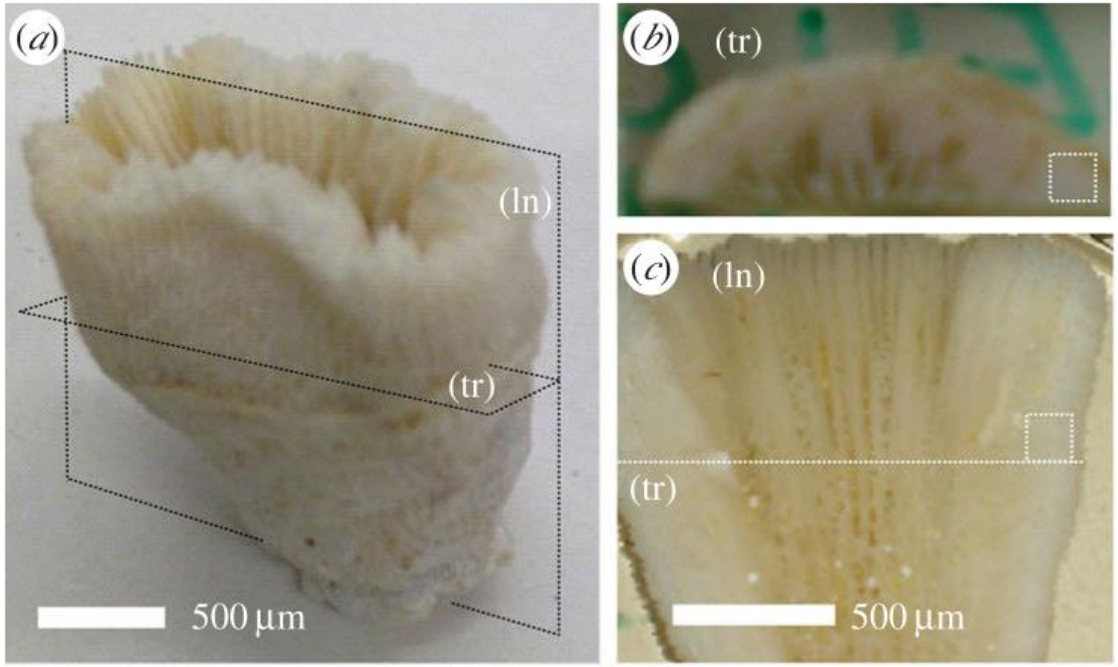

Camera pictures of the intact skeleton of *B. europaea* (a) coral showing longitudinal (ln) and transverse (tr) cutting planes with respect to the main growth axis. The mechanical properties and fiber's orientations are the same along the two sections.

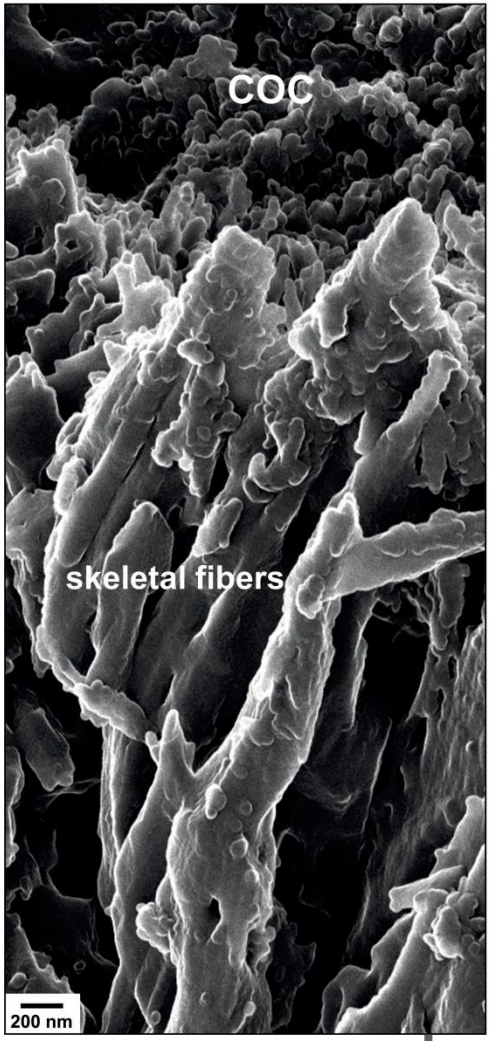

SEM micrograph from a restricted area of a trabecula composed of skeletal fibers that arise from the COC.

Coral skeletons – all sharing common feautures skeletal – distribution OM

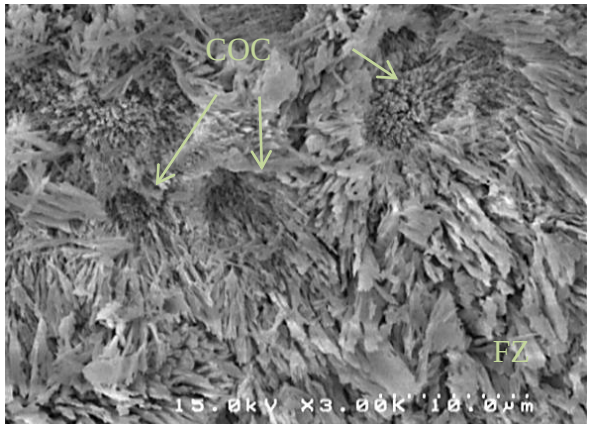

Leptopsammia pruvoti

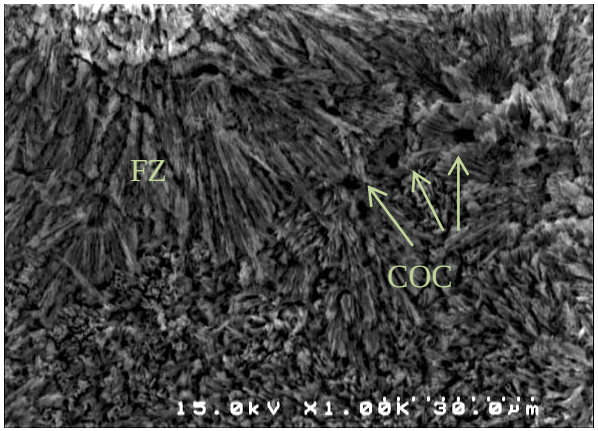

Balanophyllia europaea

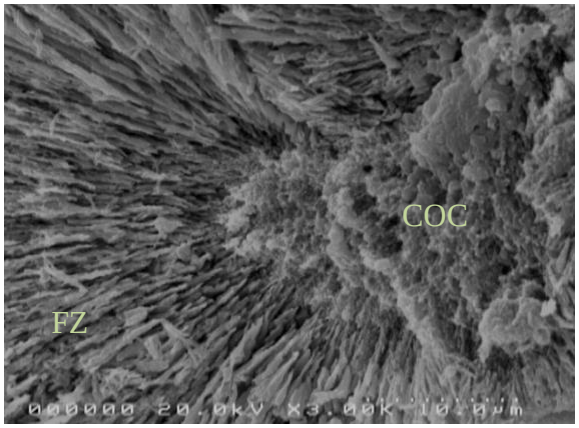

Lophelia pertusa

Despite the different growth form, colonial vs solitary, respectively, and the different morphology of the skeleton, a similar microarchitectural organization is observed.

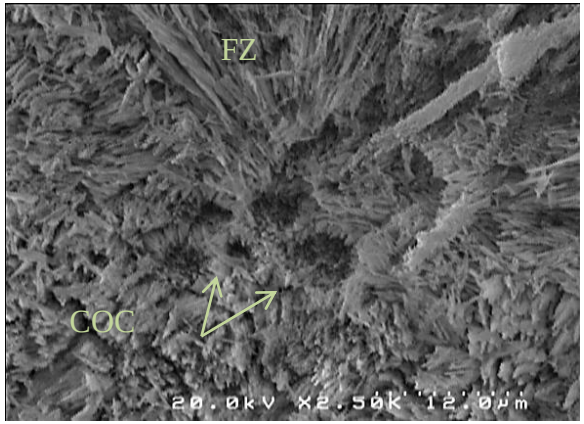

Acropora digitifera

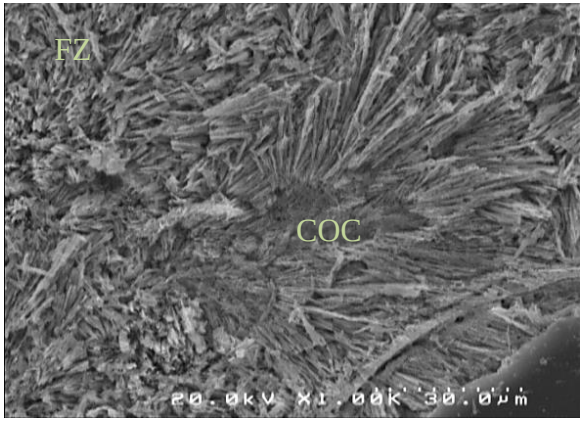

Montipora caliculata

Physio-chemical controlled mineralization

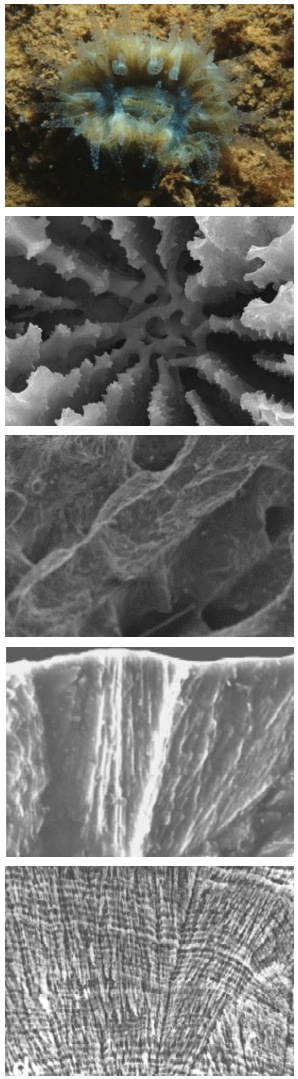

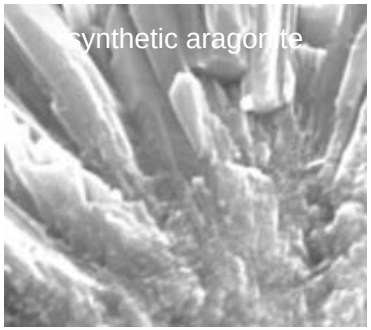

night mineralization

pH = 8; $\Omega_{ara} < 10$;

day mineralization

pH = 9; $\Omega_{ara} > 100$

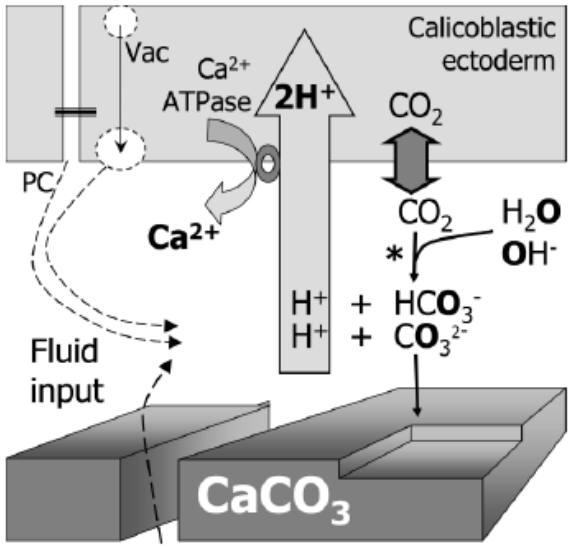

Skeletal texture differences in coral may beexplicable in terms of the light sensitive action of the Ca^{2+}-ATPase pump. Ca^{2+}-ATPase pump is turned off at night (A. Cohen).

The intra-skeletal organic matrix composition – $CaCO_3$ interaction

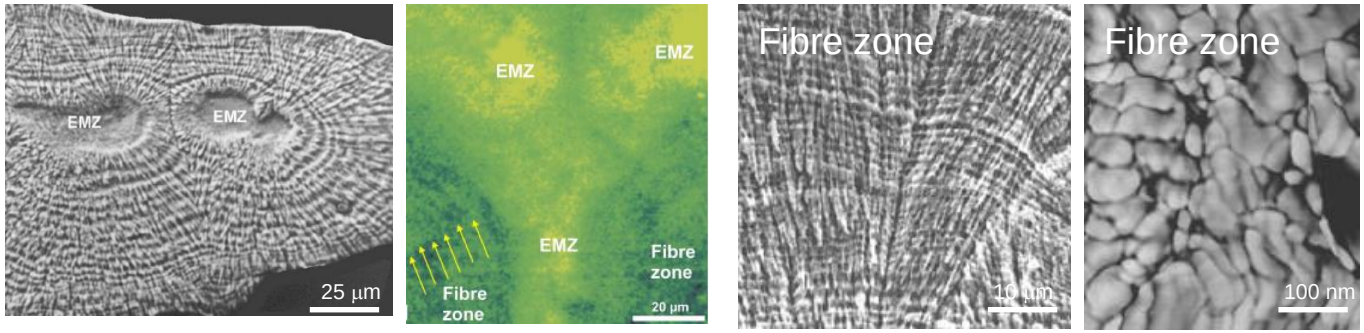

Textural features of the coral skeleton and organic matrix distribution

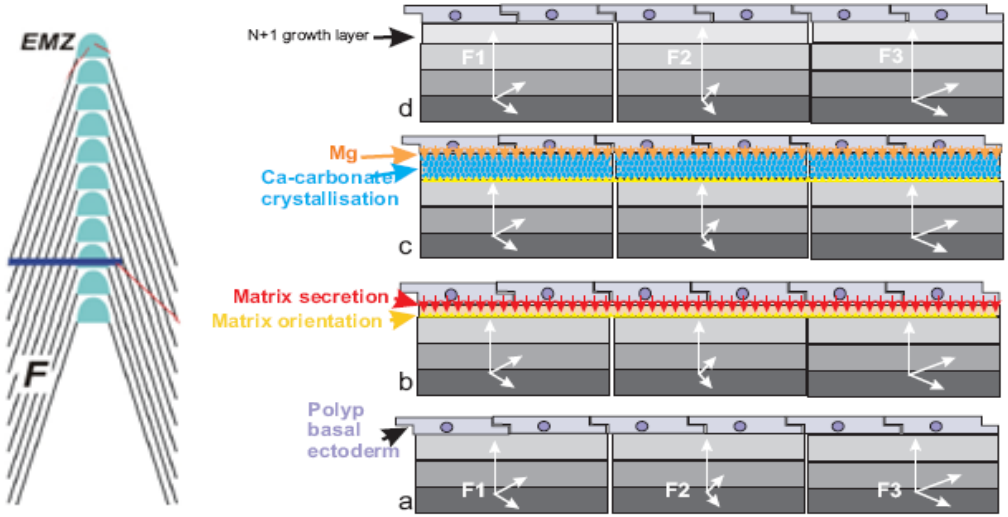

Schematic illustration of the fiber organization in the corallite and proposed mechanism for the growth of mineral layers . The OM controls the mineral deposition (Dauphin and Cuif, 2005)

Intra-skeletal Organic Matrix Components

Analytical pyrolysis-based study on intra-skeletal organic matrices

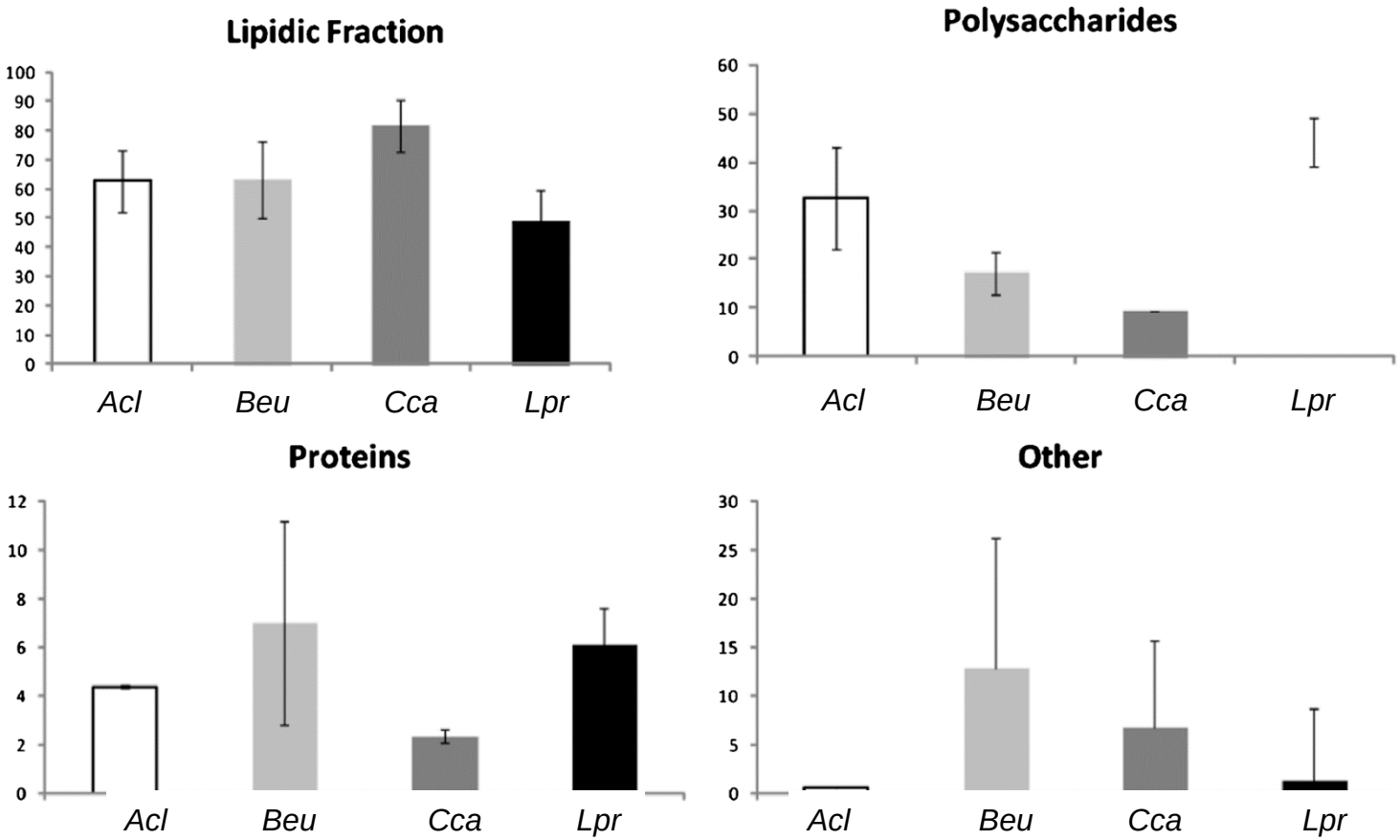

Relative percentage compositions of coral organic matters determined by Py/GC–MS calculated for each compound of the class (i) and for every identified analyte (j), as (Σi (Ai)/Σj (Aj))×100

Intra-skeletal Organic Matrix - Proteins

SDS-polyacrylamide gels electrophoresis of SOM and IOM from *B. europaea*

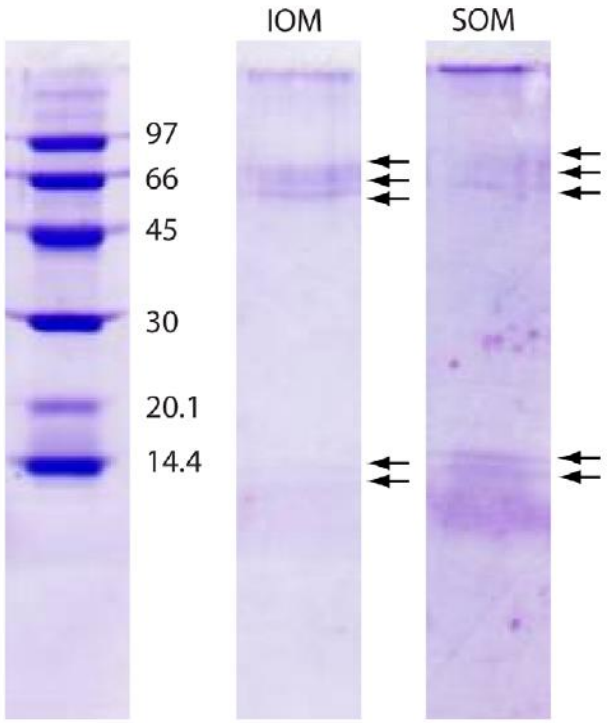

SDS PAGE according to Gotliv et al., 2003

	SOM					IOM				
	AD	LPE	MC	BEU	LPR	AD	LPE	MC	BUE	LPR
Asx	**46.8**	**31.0**	**34.9**	**46.2**	**26.6**	**17.0**	**24.7**	**13.8**	**12.6**	**17.8**
Glx	**2.4**	**3.7**	**3.6**	**6.6**	**7.6**	**2.4**	**3.3**	**5.7**	**8.3**	**9.1**
Ser	6.1	6.9	5.6	12.8	14.0	0.5	6.5	6.9	9.2	8.1
Gly	14.2	16.6	21.9	17.7	16.8	25.3	30.3	21.8	22.3	13.8
His	5.1	8.3	3.5	2.4	3.0	6.4	1.2	4.7	4.2	4.9
Thr	4.9	7.0	6.0	0.3	0.0	0.8	2.5	5.2	1.1	3.1
Arg	6.7	7.0	6.3	0.5	0.0	6.2	3.7	4.6	3.5	4.2
Ala	**1.2**	**6.4**	**4.1**	**4.1**	**5.5**	**9.2**	**7.4**	**9.0**	**13.2**	**6.5**
Tyr	6.8	2.5	1.3	0.2	-	0.5	1.9	2.6	1.9	1.7
Cys	1.0	1.0	1.0	1.0	1.0	1.0	1.0	1.0	1.0	1.0
Val	**0.4**	**1.8**	**1.4**	**2.6**	**2.4**	**3.5**	**1.3**	**3.8**	**4.8**	**5.8**
Met	-	-	-	-	-	1.0	-	-	-	-
Phe	2.4	1.7	2.3	1.1	0.6	0.9	-	7.3	3.0	-
Ile	**1.7**	**2.3**	**2.8**	**1.6**	**1.2**	**5.9**	**1.8**	**4.4**	**3.6**	**4.3**
Leu	**1.4**	**2.9**	**2.5**	**1.9**	**1.7**	**7.3**	**6.1**	**6.9**	**5.4**	**7.5**
Lys	-	2.1	3.9	0.5	-	14.3	9.3	3.3	3.2	3.4

Intra-skeletal Organic Matrix - Polysaccharides

Samples	Monosaccharide composition (%)[a]				
	Ara	Xyl	Man	Gal	Glc
Spi	6.5	5.0	6.0	2.0	80.5
Beu	4.1	3.8	7.1	7.0	78.0
Aca	3.0	4.1	7.2	5.3	80.4

Ara = arabinose; Man = mannose; Xyl = xylose;
Gal = galactose and Glc = glucuronic acid.

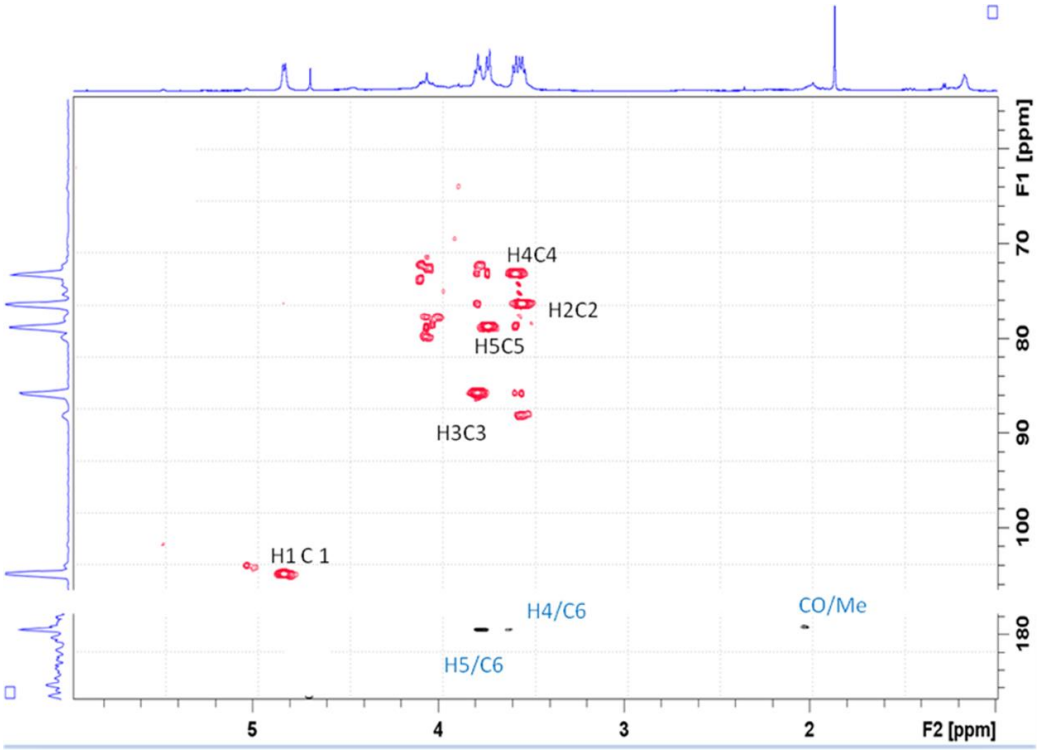

Polysaccharides represent a main weight fraction of the intraskeletal organic matrix of corals their key component is a 1→3 β-D glucuronic acid polymer

Intra-skeletal Organic Matrix - Lipids

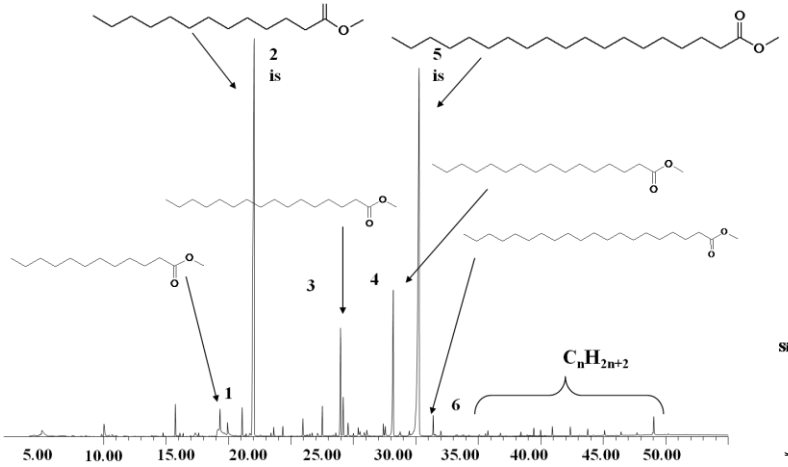

Fatty acids from methanolysis (methyl-esters)

N°	Name	RT
1	Lauric acid, methyl ester ($C_{13}H_{26}O_2$)	17.485
2	Methyl tridecanoate ($C_{14}H_{28}O_2$ **is**)	19.830
3	Palmitic acid, methyl ester ($C_{17}H_{34}O_2$)	25.938
4	Stearic acid, methyl ester ($C_{19}H_{38}O_2$)	29.635
5	Methyl nonadecanoate ($C_{20}H_{40}O_2$ **is**)	31.469
6	Ethyl nonadecanoate ($C_{21}H_{42}O_2$)	32.462

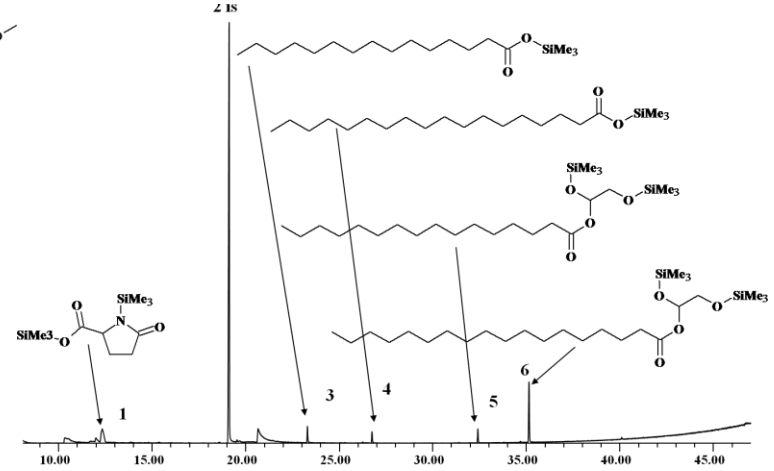

Free fatty acids (trimethylsilyl-esters)

N°	Name	RT
1	Pyro-glutammic acid (N-trimethylsilyl) trimethylsilyl ester	12.344
2	1-Benzyl-3-oxo-piperazine N-trimethylsilyl (**is**)	19.113
3	Palmitic acid , trimethylsilyl ester ($C_{19}H_{40}O_2Si$)	23.302
4	Stearic acid, trimethylsilyl ester ($C_{21}H_{44}O_2Si$)	26.746
5	1-Monopalmitoylglycerol trimethylsilyl ether ($C_{25}H_{54}O_4Si_2$)	32.400
6	Stearic acid, 2,3-bis(trimethylsiloxy)propyl ester ($C27H_{58}O_4Si_2$)	35.129

The lipid composition observed in *B. europaea* is in agreement with what of those extracted from other zox coral species and mollusc shells.

Intra-skeletal Organic Matrix - Lipids

Content (wt‰) and composition (wt%) of FA extracted from the coral skeleton from *A. calycularis* (ACL), *B. europaea* (BEU) and *S. pistillata* (SPT)..

FA	ACL	BEU	SPT
Content	0.7 ± 0.5	1.0 ± 0.5	1.1 ± 0.8
Composition			
C14:0	3.9 ± 0.9	6.1 ± 2.4	2.6 ± 0.7
C15:0	4.5 ± 2.7		
C16:0	51.0 ± 2.6	52.4 ± 1.6	47.5 ± 1.3
C17:0	4.6 ± 0.6		
C18:1	—	14.7 ± 1.6	8.1 ± 3.2
C18:0	42.6 ± 1.8	29.5 ± 1.7	41.8 ± 1.5

*lip*OM, only when dispersed at a concentration of 100 μg mL^{-1} in the 10 mM $CaCl_2$, assembled in particles having hydrodynamic radii of 239.5 ± 7.4 nm and 232.5 ± 7.1 nm for *A. calycularis* and *S. pistillata*, respectively, and of 169.9 ± 6.7 nm for *B. europaea*.

In vitro $CaCO_3$ precipitation - synthetic strategies -

Overgrowth experiments

(+) minimally affect the native state of macromolecules

(-) not all intra-skeletal macromolecules can be released

In solution experiments

(+) allow to study the effects of a single additive

(-) not representative of physiological conditions

Kinetics studies by overgrowth experiments

(+) allow to control the role of supersaturation

(-) the adsorbed macromolecules are not representative of the whole organic matrix

Counter diffusion in gels

(+) allows to investigate a high number of supersaturation conditions

(+) biomineralization occurs in a gelling environment

(-) not easy to measure key variables

In vitro $CaCO_3$ precipitation by overgrowth

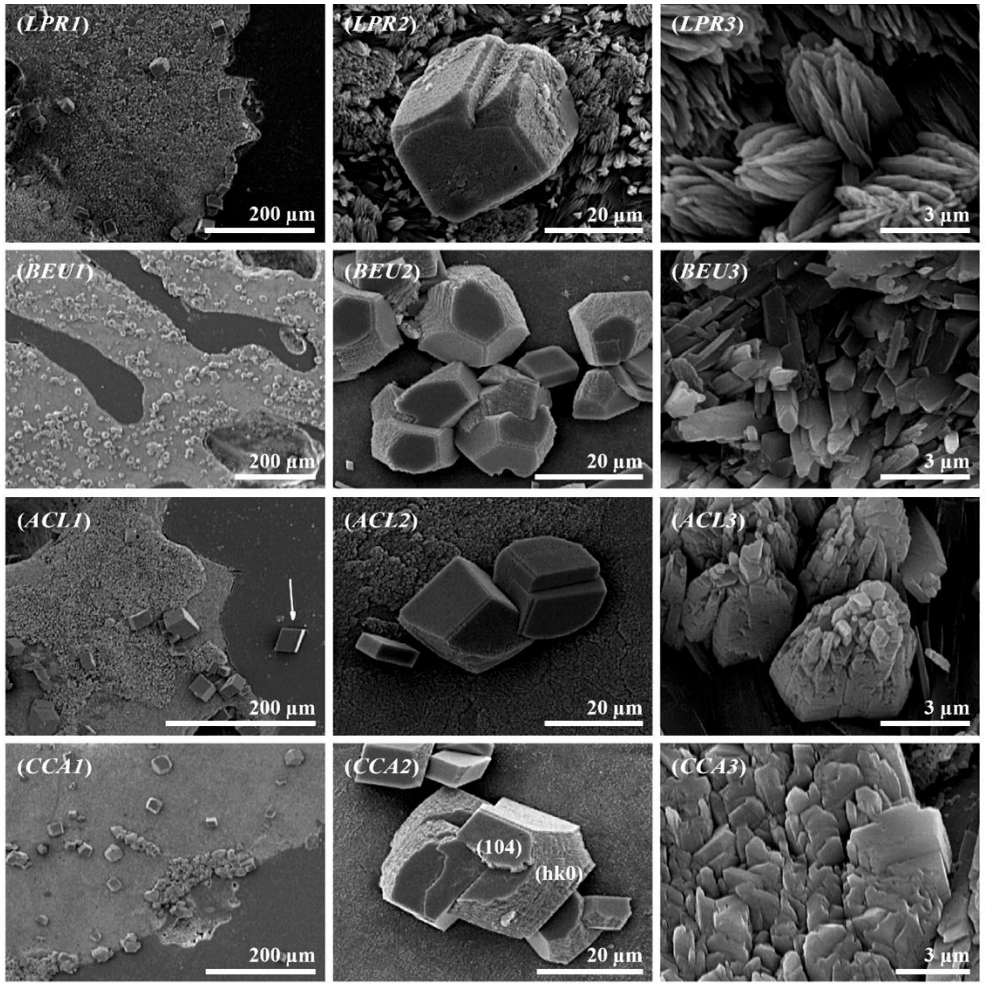

Overgrowth experiment

- OM components stabilize aragonite growth
- Crystals have specie specific size and texture
- OM macromolecules interact with calcite crystals
- Only Ca^{2+} in solution

SEM pictures at increasing magnifications (1–3) of sections of coral skeleton of *A. digitifera* (*AD*), *L. pertusa* (*LPE*), *M. caliculata* (*MC*), *B. europaea* (BEU), *L. pruvoti* (LPR), *A. calycularis* (ACL) and *C. caespitosa* (CCA) after the calcium carbonate overgrowth experiment

In vitro $CaCO_3$ homogeneous precipitation

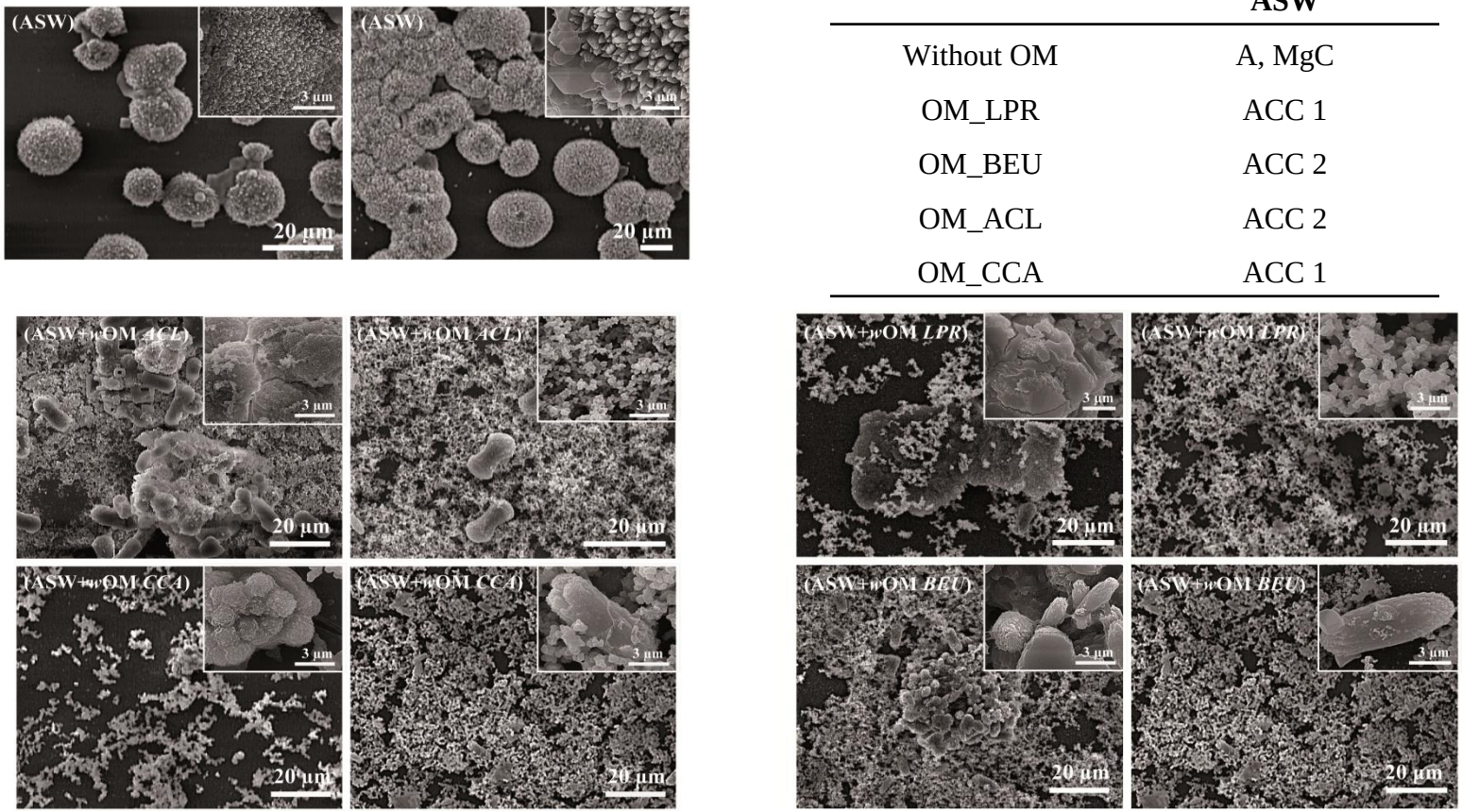

	ASW
Without OM	A, MgC
OM_LPR	ACC 1
OM_BEU	ACC 2
OM_ACL	ACC 2
OM_CCA	ACC 1

SEM pictures of particles obtained from precipitation experiments of $CaCO_3$ from artificial sea water (ASW) in the presence of the entire organic matrix (OM). The OMs were extracted from *L. pruvoti* (LPR), *B. europaea* (BEU), *A. calycularis* (ACL) and *C. caespitosa* (CCA), respectively. These pictures are the most representative of the populations of observed particles.

In vitro $CaCO_3$ homogeneous precipitation

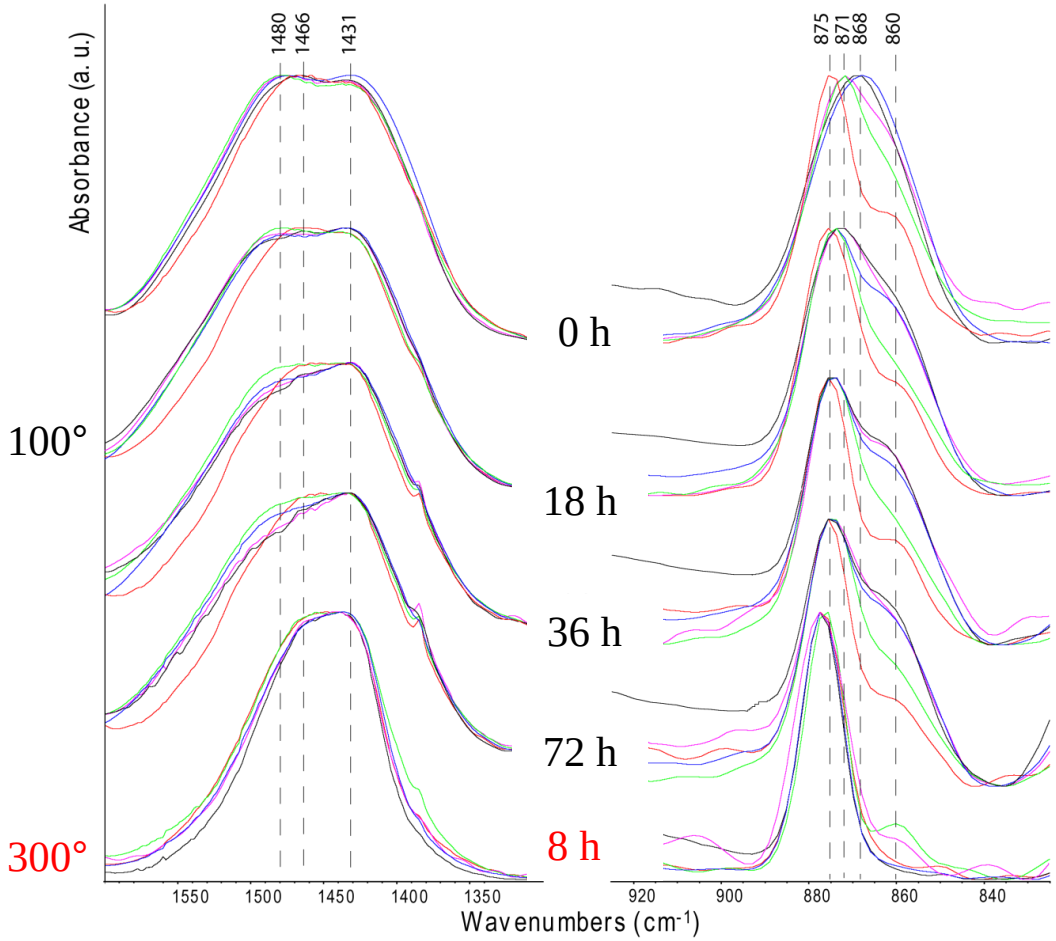

FTIR spectra of calcium carbonate precipitated from artificial sea water in the presence of the *e*OM, which was extracted from *L. pruvoti* , *B. europaea*, *A. calycularis* and *C. caespitosa*. The spectra from calcium carbonate precipitated from artificial sea water in the absence of *e*OM are also reported (red).

The presence of two forms of ACC were detected

(PUPA Gilbert)

In vitro $CaCO_3$ precipitation - kinetics studies

Spontaneous precipitation experiments using ASW1 with initial pH_0 = 10.2

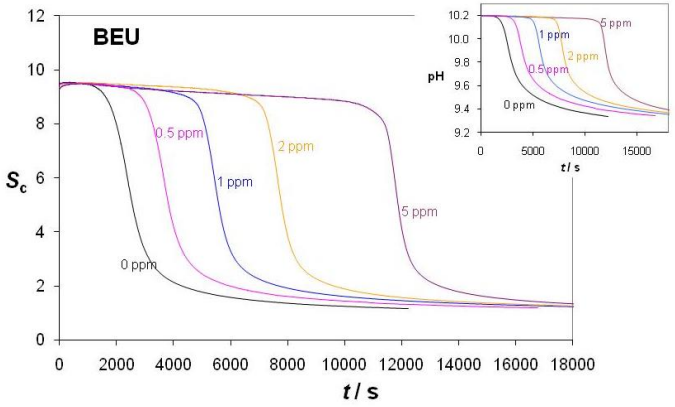

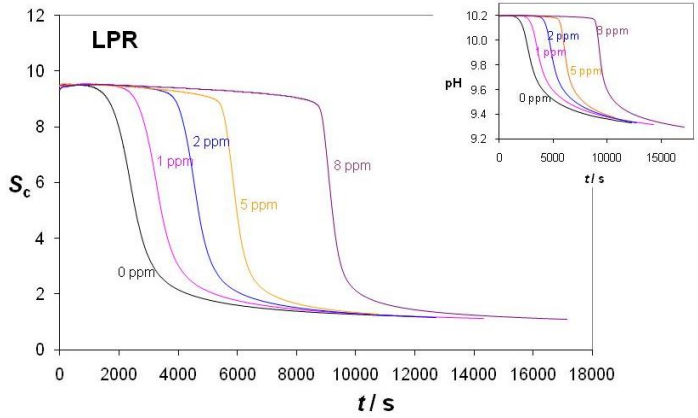

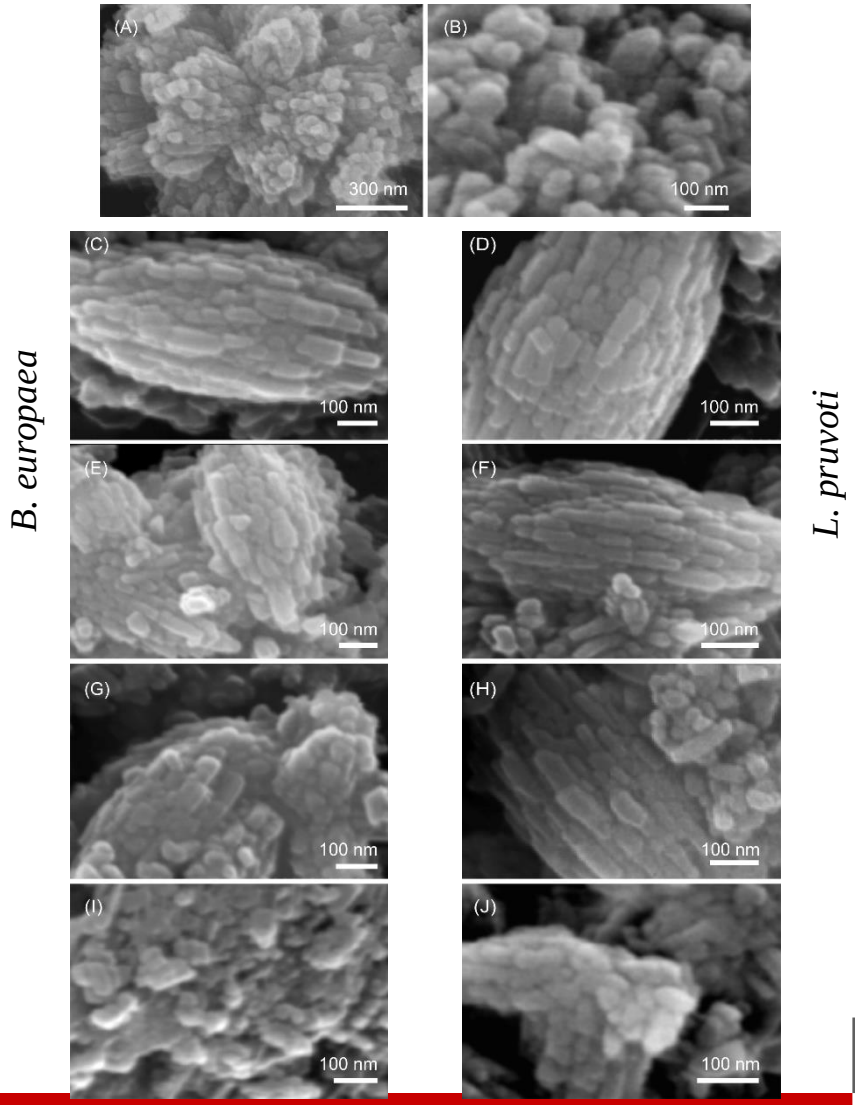

The *in vitro* $CaCO_3$ precipitation - kinetics studies by overgrowth -

Seeded precipitation experiments using ASW2 with initial pH_0 = 9.0

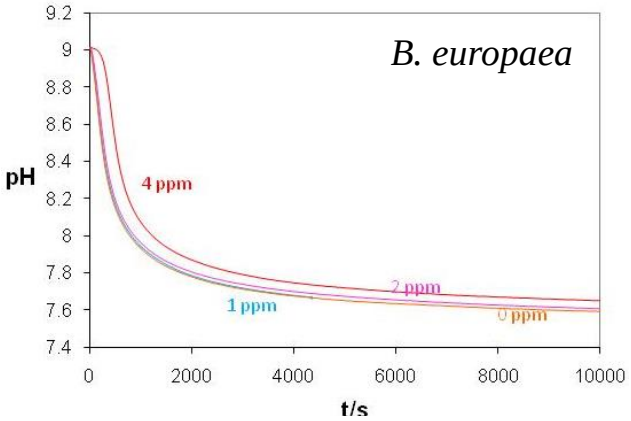

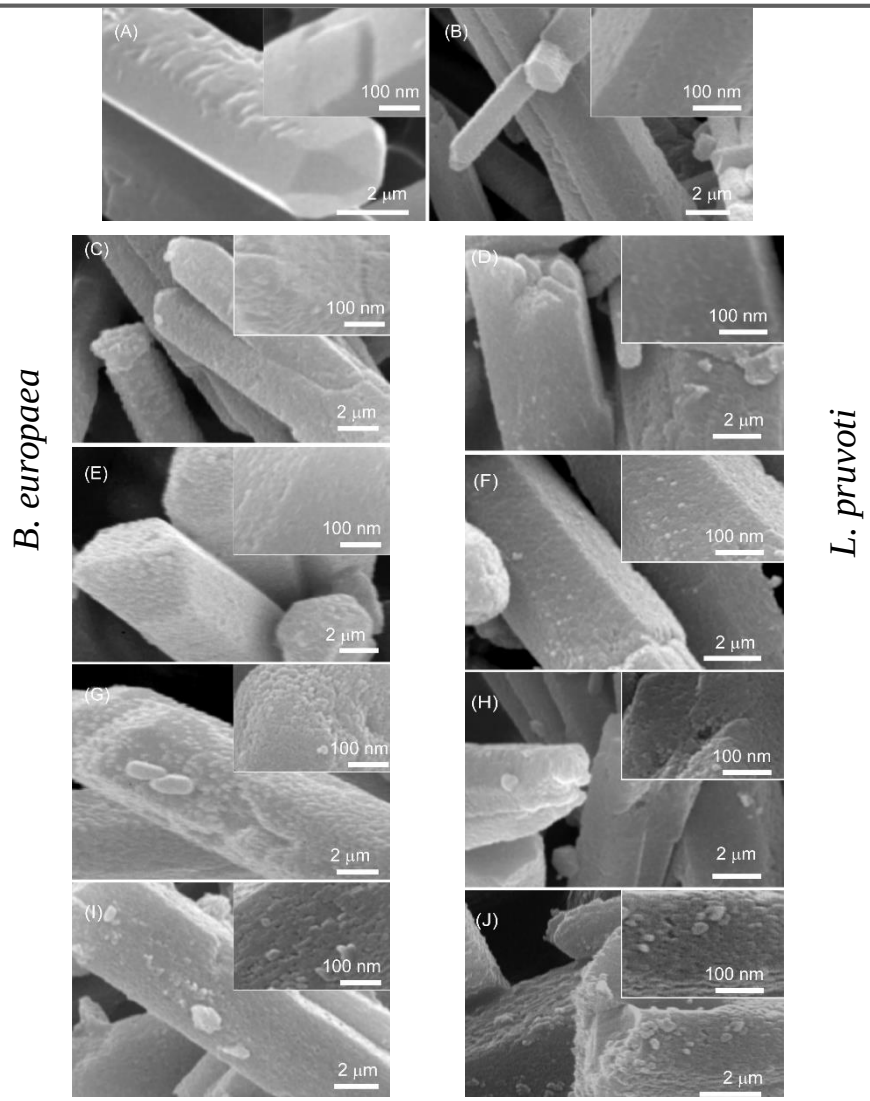

In vitro $CaCO_3$ precipitation – gel CDS

COUNTER DIFFUSION SYSTEM (CDS)
represents a scenario with physical and ion-transport characteristics close to that occurring *in vivo*

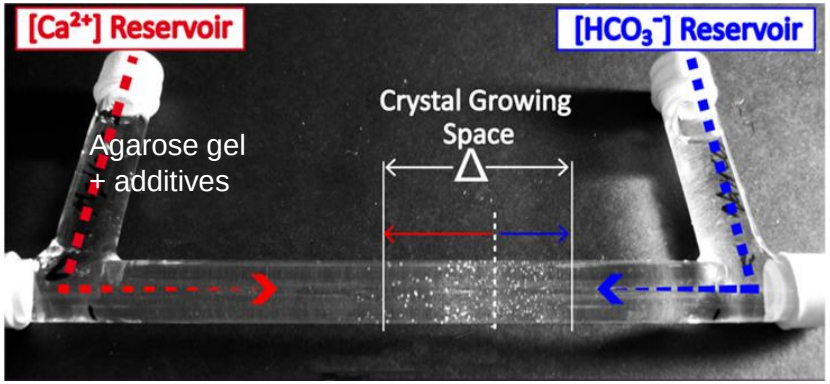

Additives can be entrapped into the gel:

1) poly-L-Aspartate (pAsp)
2) SOMs extracted from coral skeletons

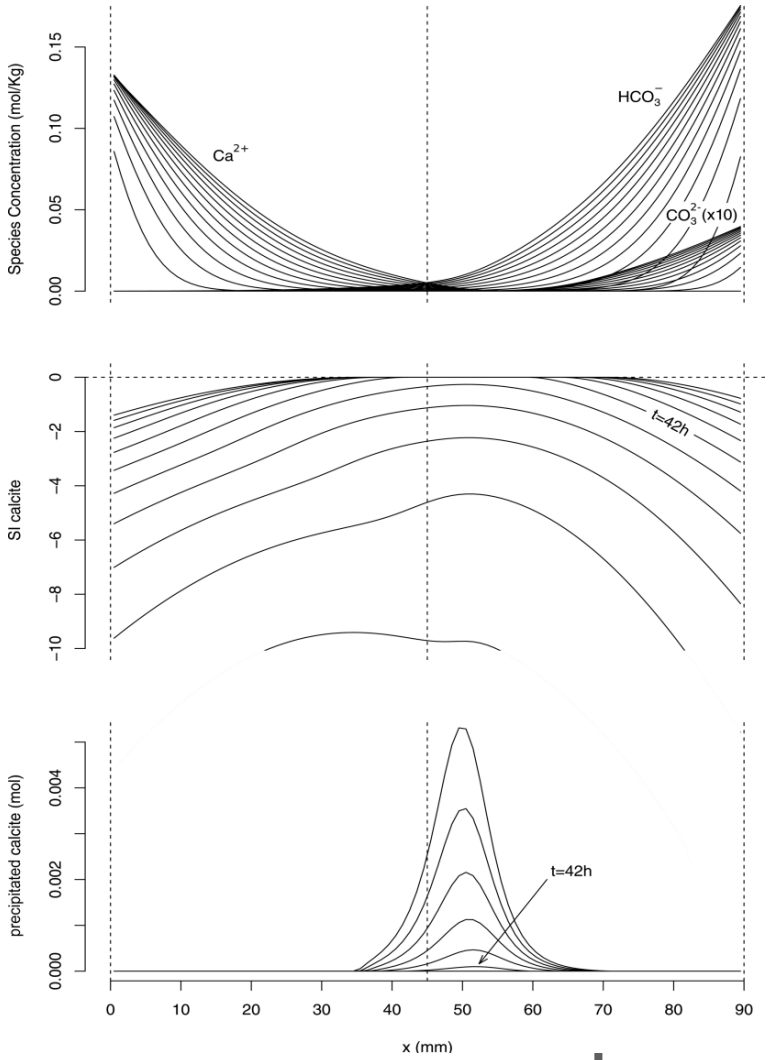

In vitro $CaCO_3$ precipitation – gel CDS

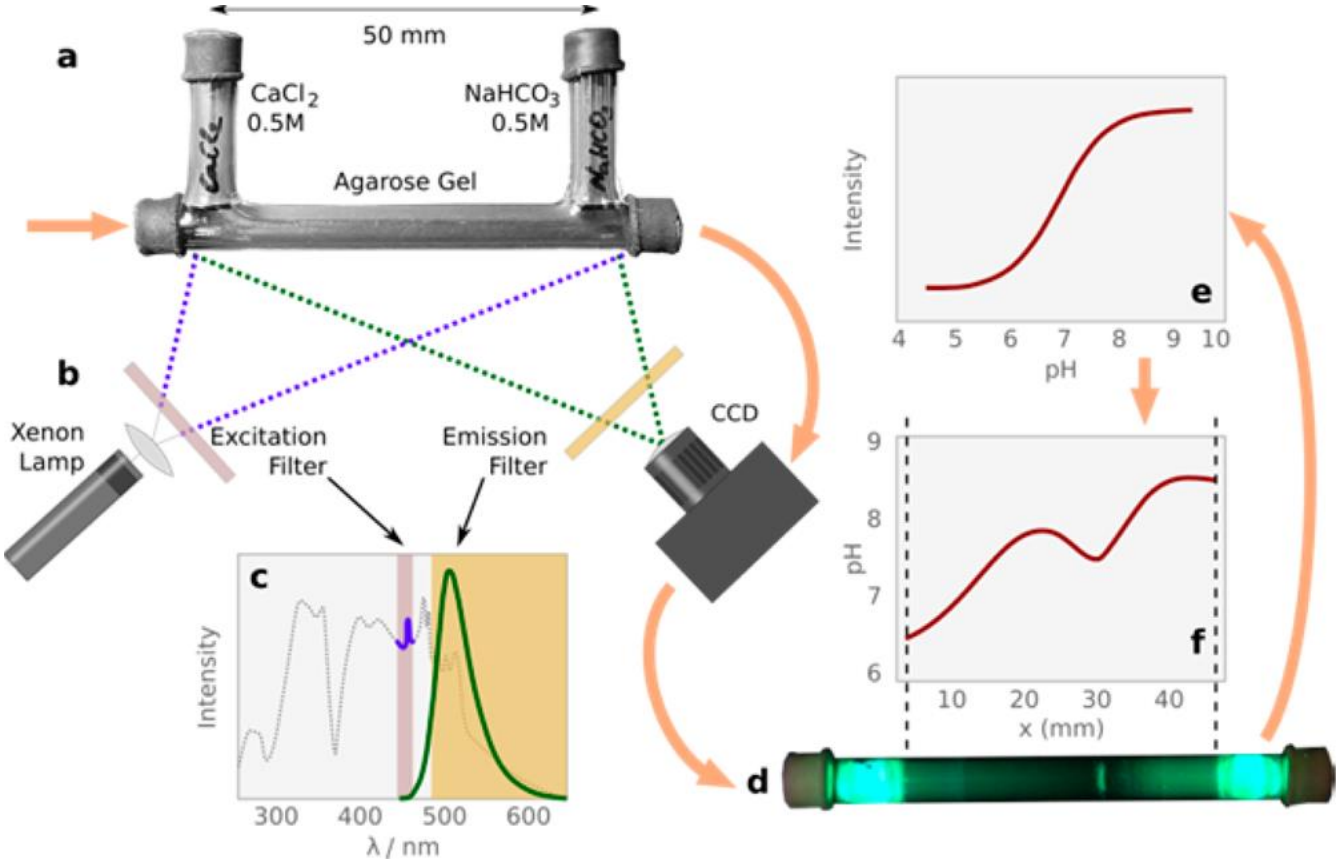

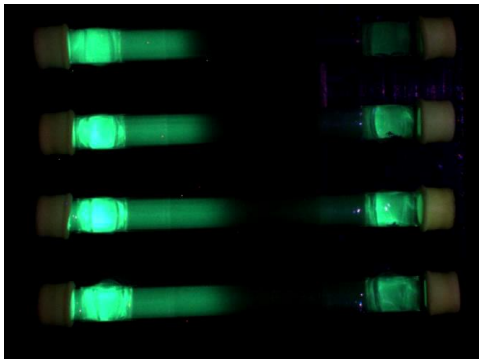

A radiation 450 nm excites green fluorescence that is imaged on a CCD. Raw fluorescence image as collected by the CCD. These images are analyzed to produce the final pH profile.

In vitro $CaCO_3$ precipitation – gel CDS

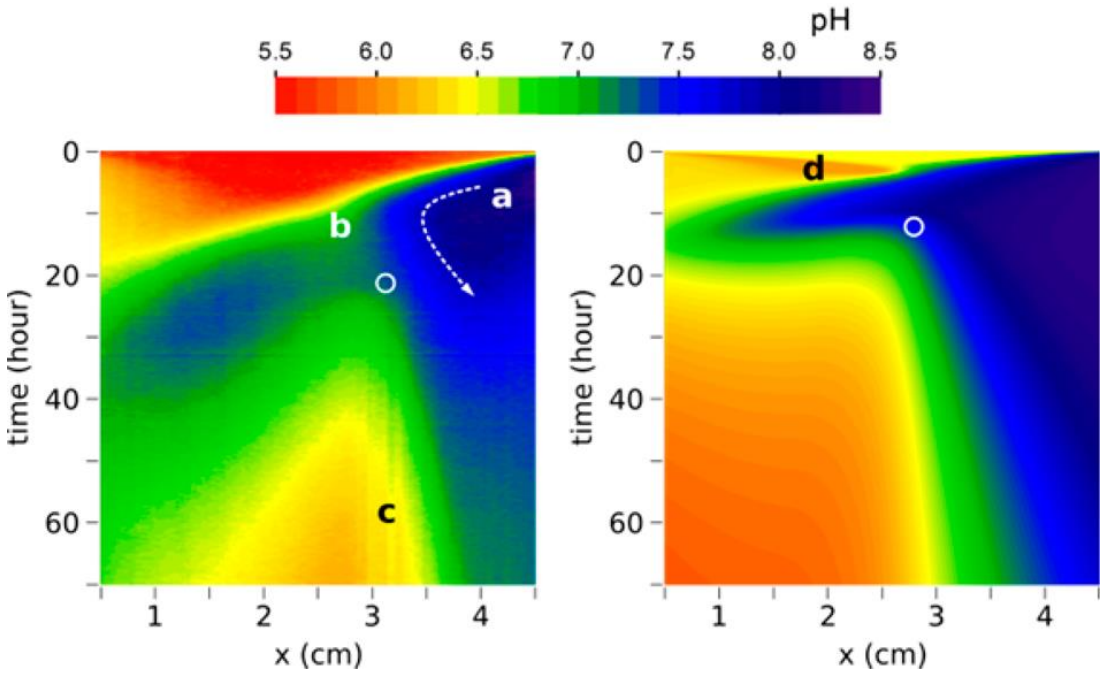

Experimental (left) and calculated (right) maps of pH−space−time.

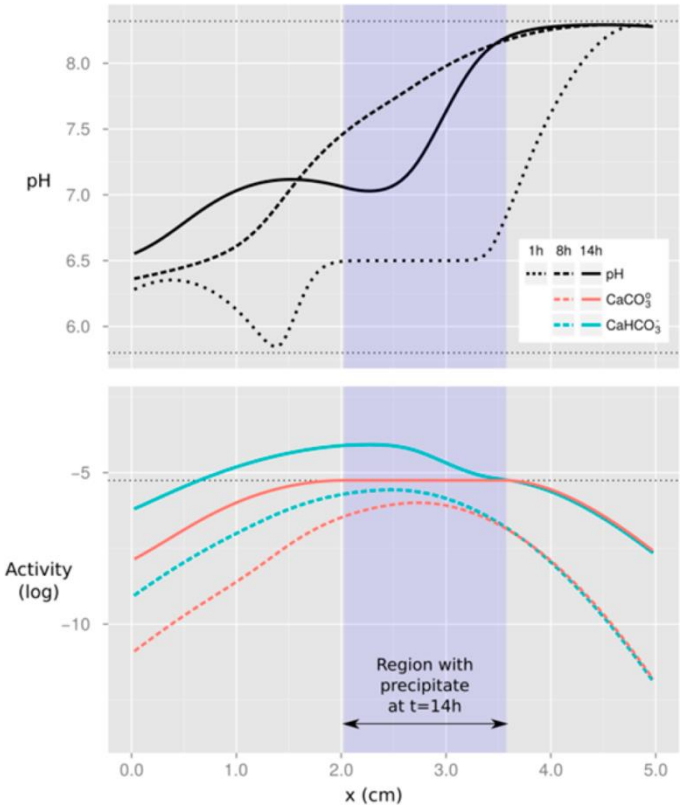

Evolution in time of pH (black lines) and activities of $CaHCO_3^+$ (blue lines) and $CaCO_3°$ (orange lines) along the gel tube. For the sake of clarity only plots after 1 h (dotted lines), 8 h (dashed lines), and 14 h (continuous lines) are shown.

$$Ca^{2+} + CO_3^{2-} \leftrightarrow CaCO_3° \qquad \log K_{CaCO_3°} = 3.22$$

$$Ca^{2+} + HCO_3^- \leftrightarrow CaHCO_3^+ \qquad \log K_{CaHCO_3^+} = 1.11$$

$$HCO_3^- \leftrightarrow CO_3^{2-} + H^+ \qquad \log K_2 = -10.33$$

$$CaHCO_3^+ \leftrightarrow CaCO_3° + H^+ \qquad \log K = -8.22$$

In vitro $CaCO_3$ precipitation – gel CDS

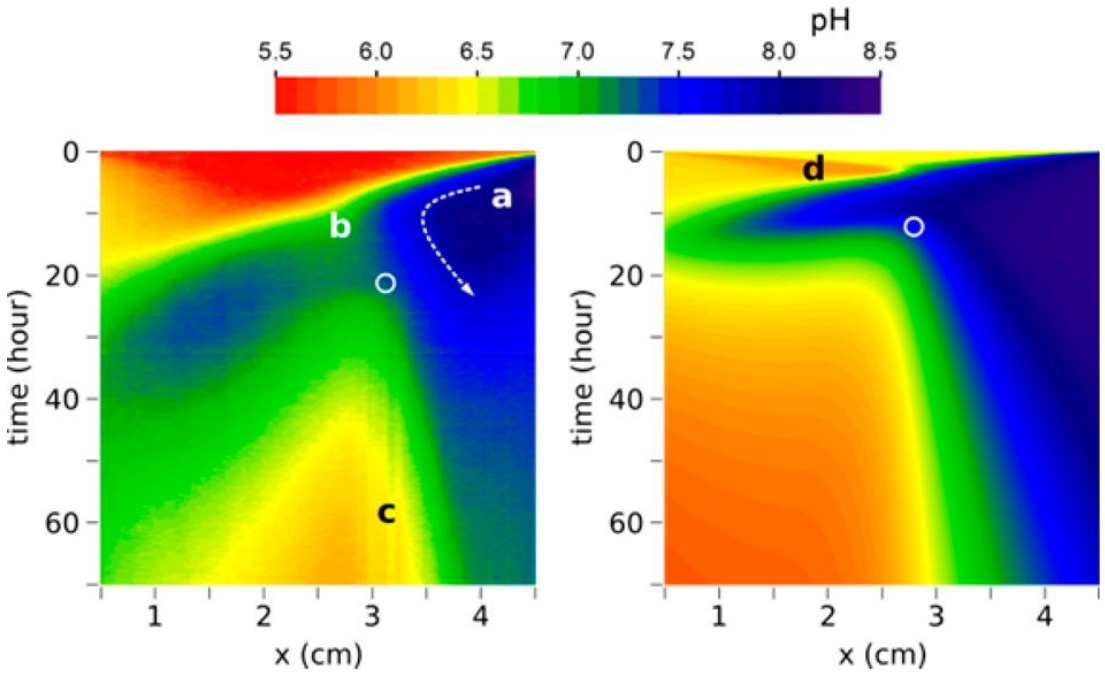

Experimental (left) and calculated (right) maps of pH−space−time..

$$CaCO_3^\circ \leftrightarrow (CaCO_3)_x \leftrightarrow CaCO_3(s)$$

with $x = 1, 2, 3, \ldots, n$

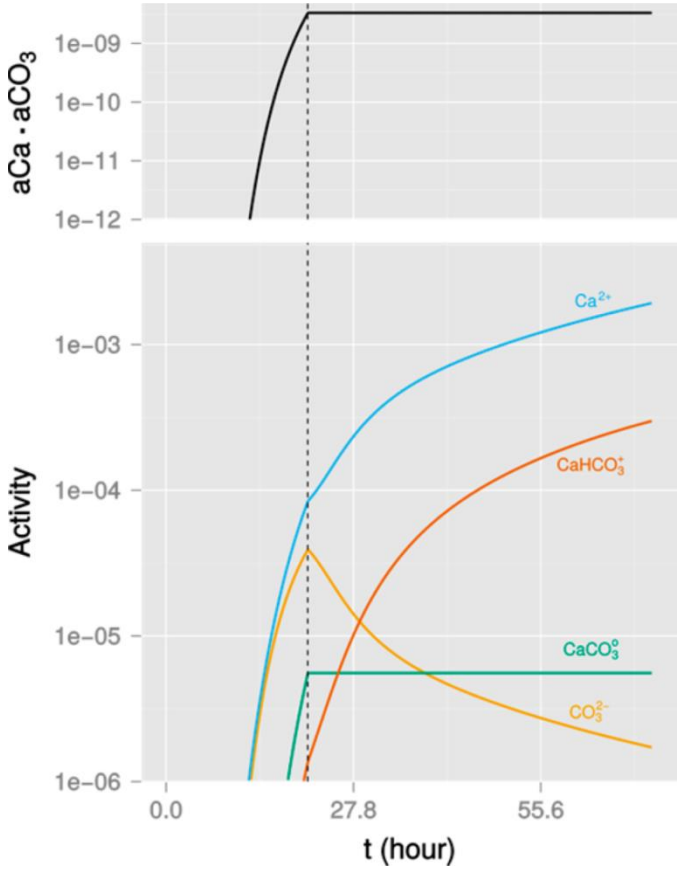

Time evolution of activity for the ions Ca^{2+}, CO_3^{2-} and the pairs $CaHCO_3^+$, $CaCO_3^\circ$ (bottom). The ionic activity product $a(Ca^{2+})$ $a(CO_3^{2-})$ is shown in the top panel.

In vitro $CaCO_3$ precipitation – gel CDS + SOM *B. europaea*

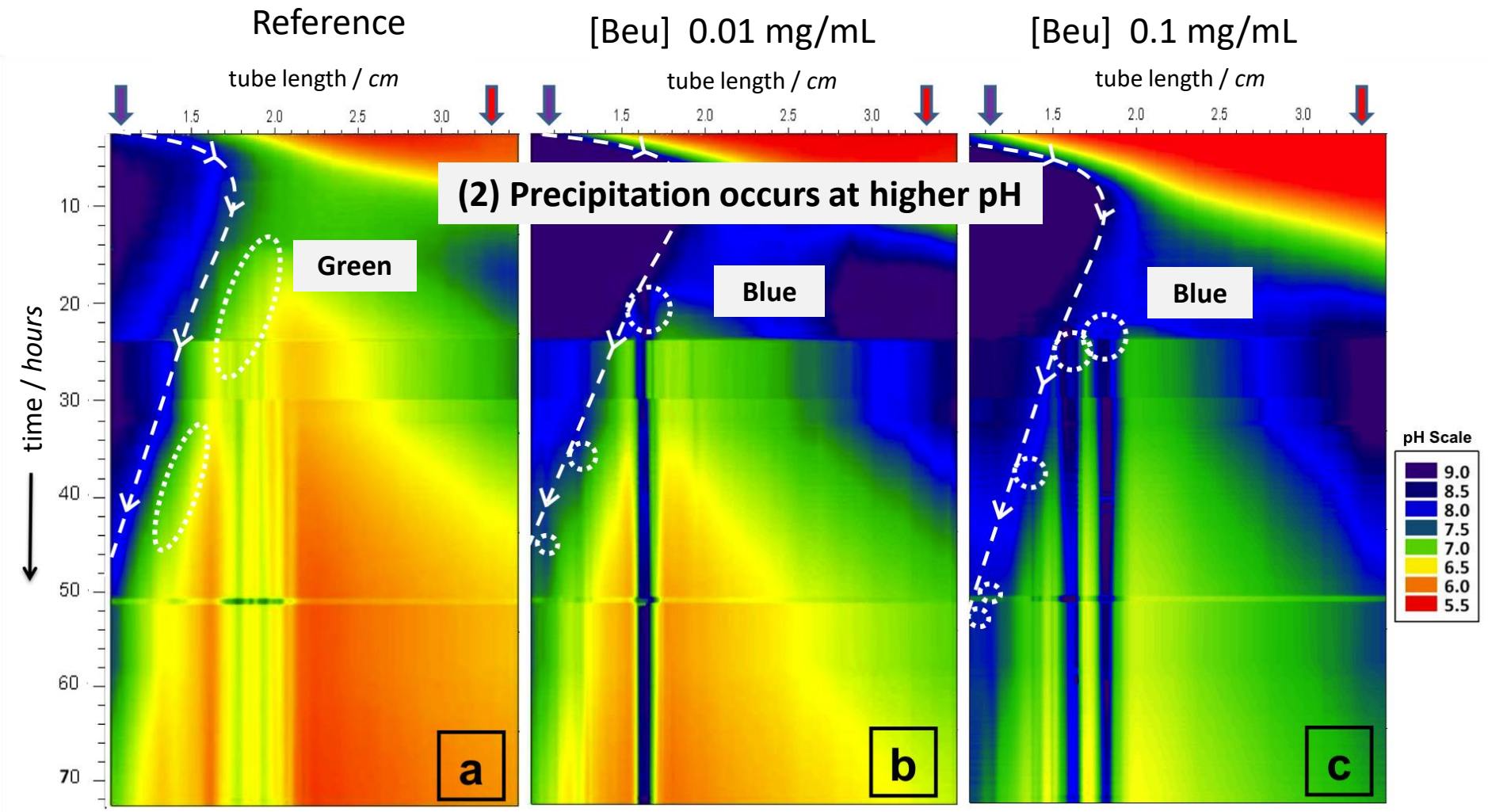

Coral biomineralization

Organic matrix controls mineral deposition

In vitro precipitation of $CaCO_3$ in the presence of intra-skeletal organic matrix macromolecules

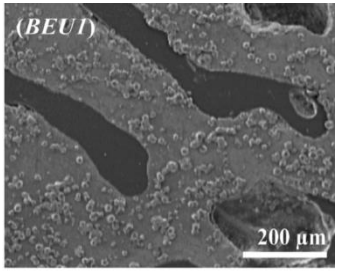

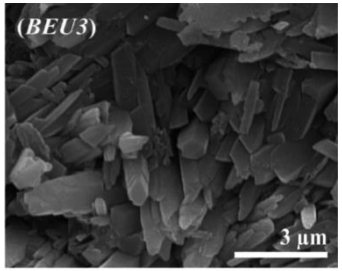

Overgrowth experiments

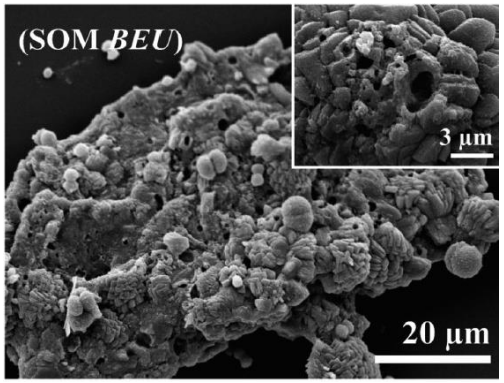

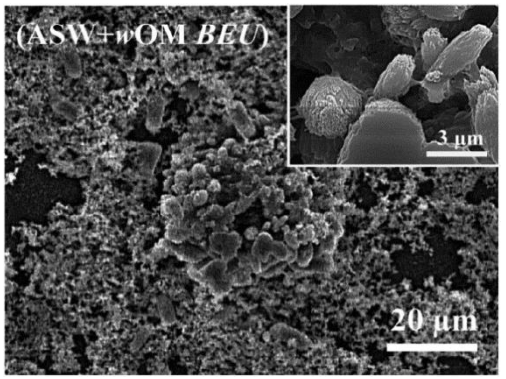

Homogeneous precipitation

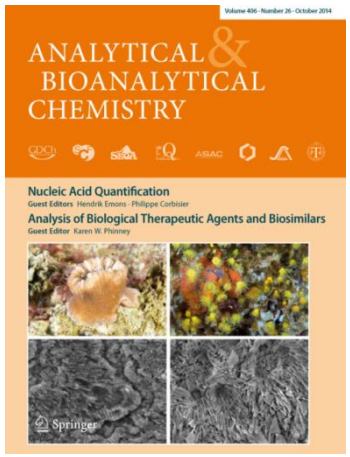

D. Kralj et al. *Chem Eur J* (2019), in press

M. Reggi et al. *ACS Omega* (2018), 3, 2895

M. Reggi et al. *CrystEngComm* (2016), 18, 8829–8833

G. Falini, et al. *Sem. Cell Developmen. Biology* (2015) 46, 17-26

A. Adamiano et al. *Anal Bioanal Chemi* (2014) 406, 6021–6033.

pH responsive drug delivery system: Calcite/Doxorubicin hybrid crystals

Calcite / Doxorubicine

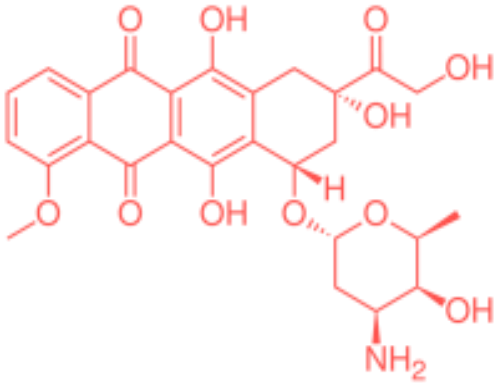

- biocompatible and biodegradable
- pH-sensitive material (enhance the bioavailability of drug in tumor tissue)
- controlled release of drug (reductions of side effects)

Calcite/DOX hybrid single crystals

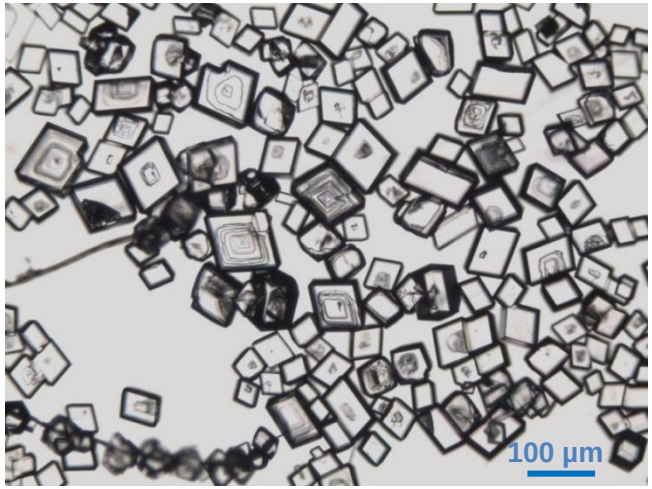

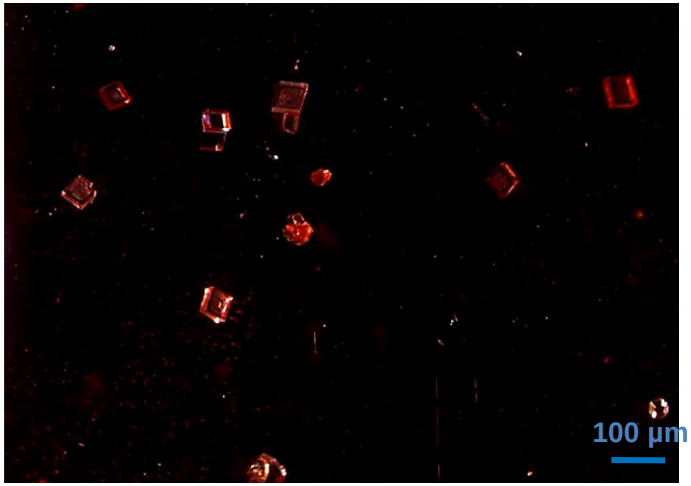

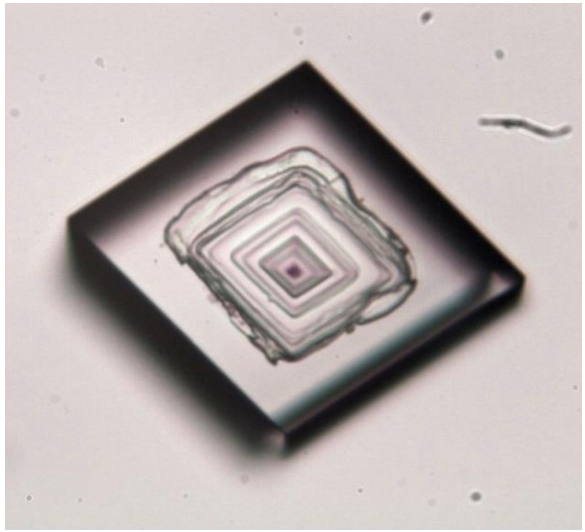

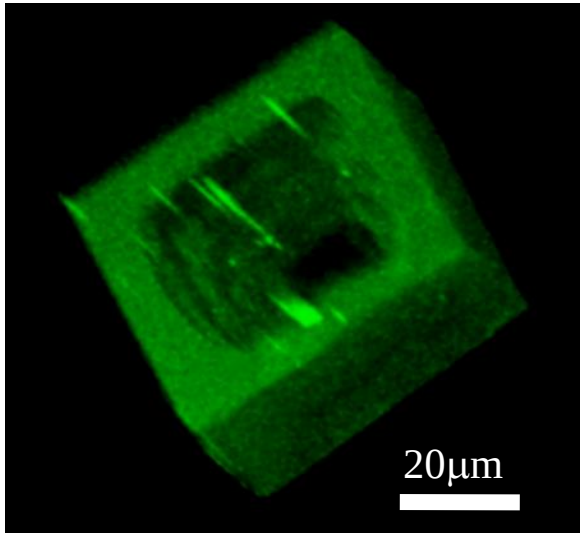

Calcite/DOX

DL 0.25% w/w

In Vitro Test

Calcite

72 h

Calcite/DOX

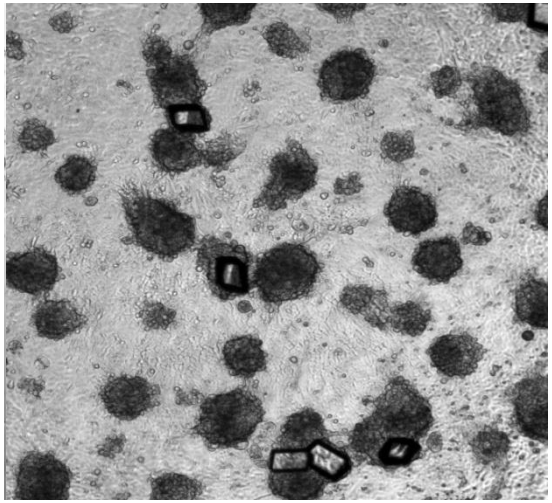

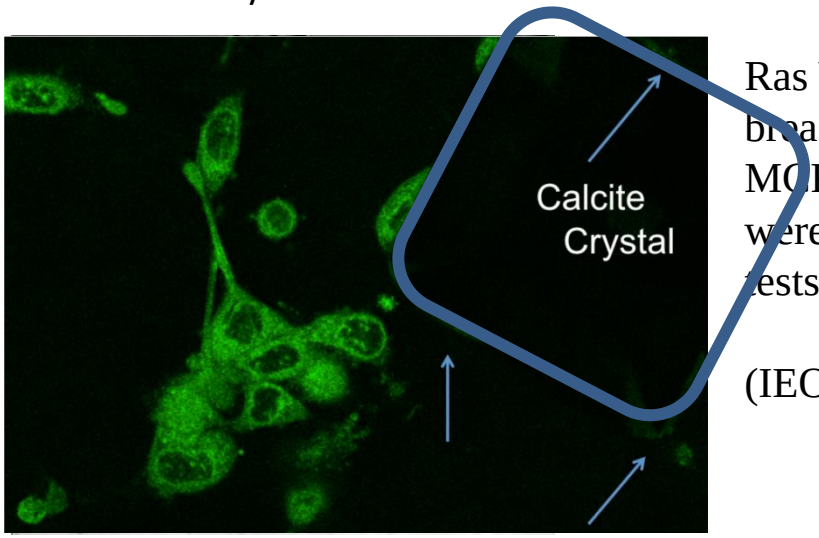

Ras V12 transformed breast epithelial MCF10A cells were used in *in vitro* tests

(IEO, Milan)

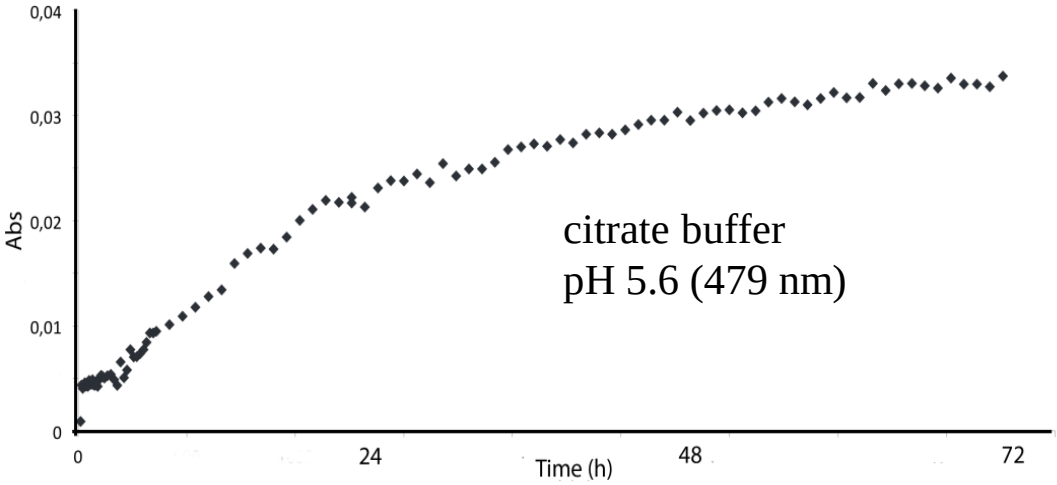

citrate buffer
pH 5.6 (479 nm)

At pH 7.4 in PBS buffer there was not detectable release of DOX

Carbon Allotropes / Calcite Hybrids

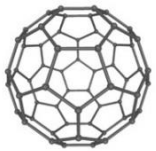

(0D) Fullerene

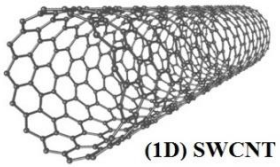

(1D) SWCNT

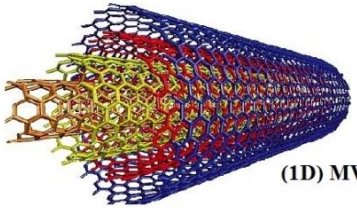

(1D) MWCNT

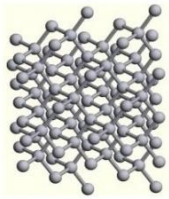

(3D) Diamond

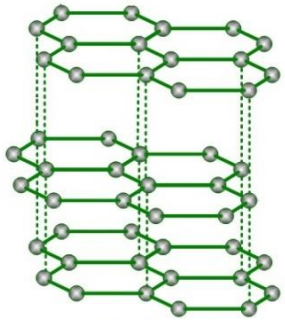

(3D) Graphite

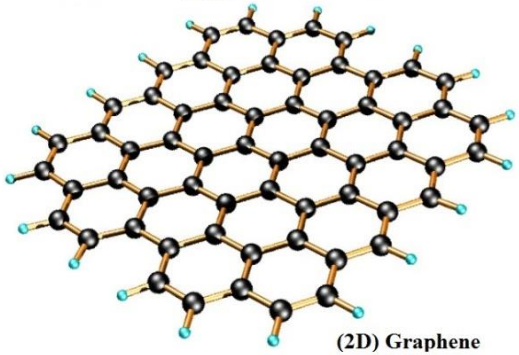

(2D) Graphene

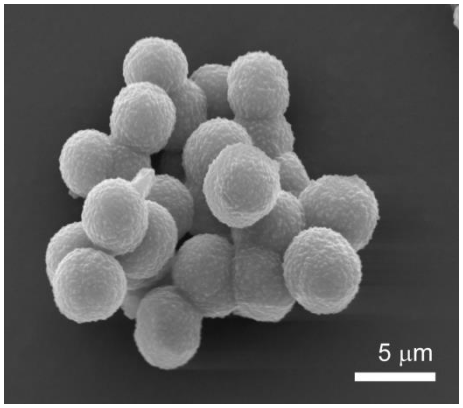

Fullerenol / calcite hybrid spheres

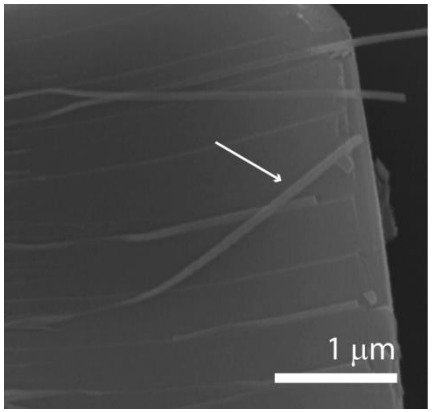

MWCN-COOH / calcite hybrid

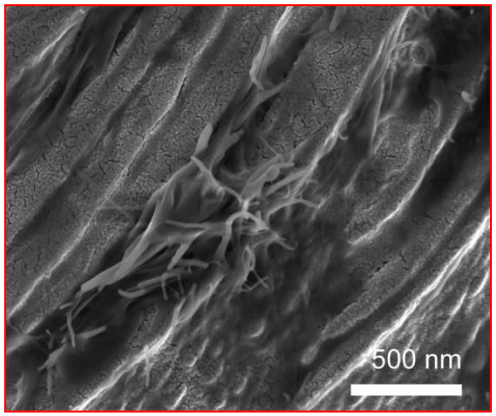

Graphene oxide / calcite hybrid

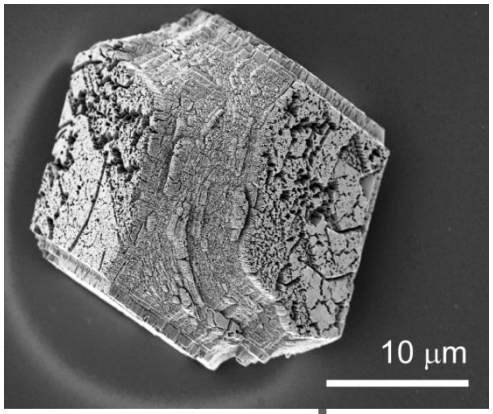

TRY-graphene / calcite hybrid

Calcite/GO hybrid single crystals

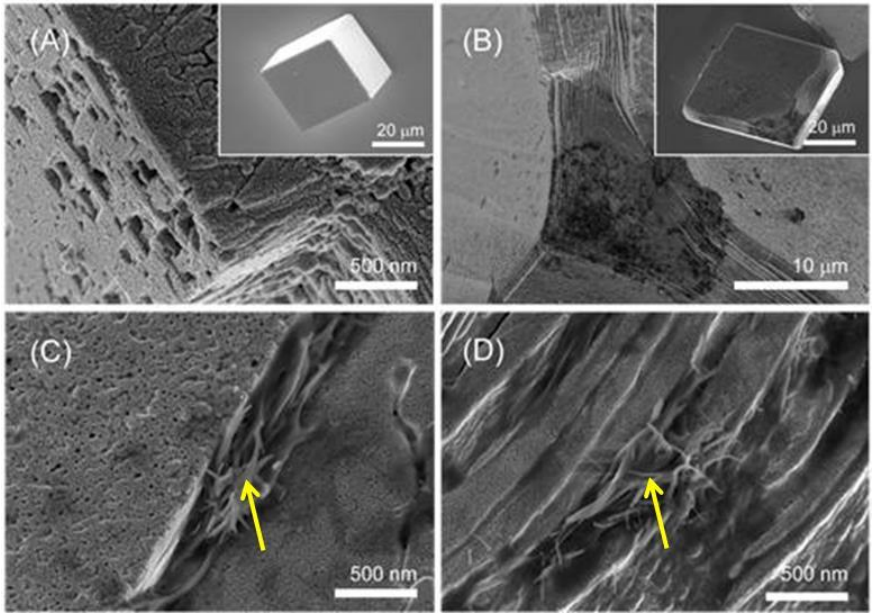

Representative HRSEM images of calcite single crystals. (A) Pure calcite (B−D) Calcite /GO hybrid single crystal.

HAADF-STEM image (A) of calcite with embedded GO sheets appearing as dark stripes, and (B) of pure calcite showing no Z-contrast.

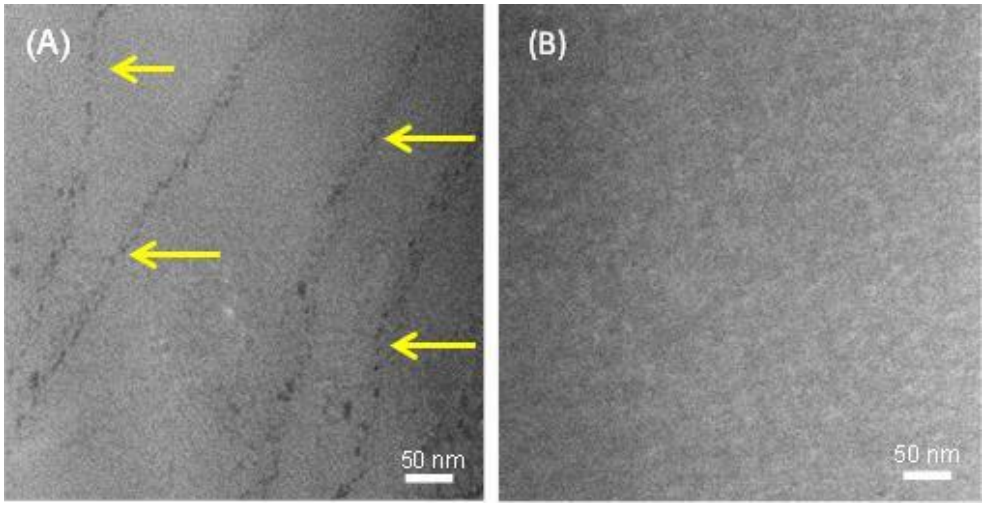

Calcite/GO hybrid single crystals

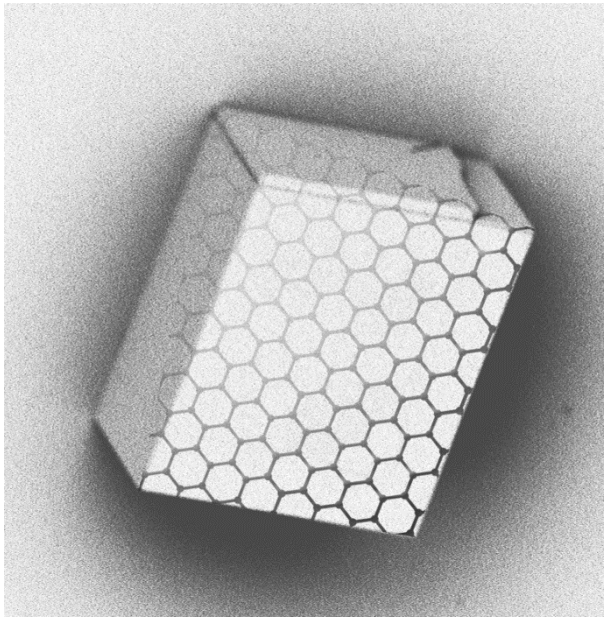

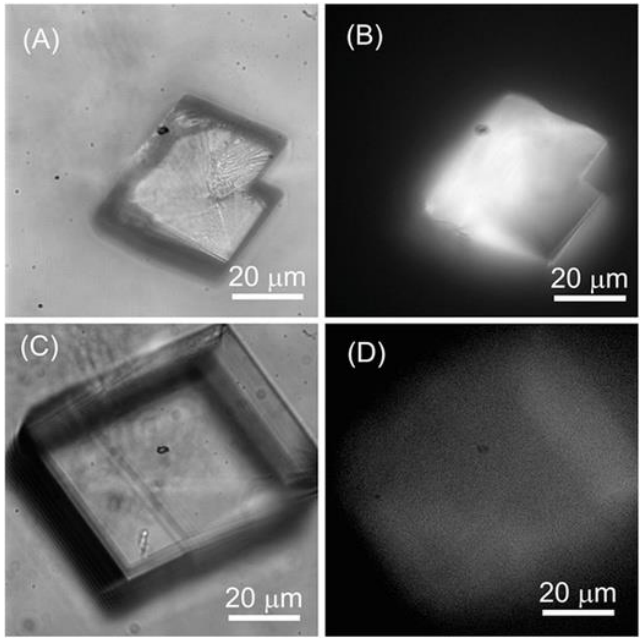

Transmission optical images of calcite crystals grown in the presence (A) and in the absence (C) of GO. On the right (B and D) are the corresponding transmission fluorescence images upon excitation at 405 nm.

Material	E_{IT} (GPa)			H_{IT} (GPa)		
	200	300	400	200	300	400
GO/calcite	59.3±4.5	55.7±3.4	53.3±3.7	4.40±0.84	4.12±0.85	4.16±0.89
Calcite	67.3±2.7	63.9±2.3	61.2±2.4	3.82±0.42	3.70±0.49	3.72±0.53
Δ%	**−11.9**	**−12.8**	**−12.8**	**15.0**	**11.4**	**11.9**

Acknowledgments

Images of university students from Lucio de Luzzi tombstone, San Vitale and Agricola church, Bologna, Italy (XIV century).

Ruđer Bošković Institute
Damir Kralj
Branka Njegic Dzakula

Technion - Israel Institute of Technology
Boaz Pokroy
Iryna Polishchuk

Consejo Superior de Investigaciones Científicas
JuanManuel Garcia Ruiz
Jaime Gomez Morales
Maria Sancho Tomas

Harvard University
James Weaver

GRAPHENE FLAGSHIP
erc
CORAL warm
HEIDELBERGCEMENT
Italcementi
Italcementi Group
PolyCrystalLine
experts in crystal forms

Biocrystallography and Biomineralization . . . . @UniBo

- **Giuseppe Falini** – **Simona Fermani** – Matteo Calvaresi -
Michela Reggi - Devis Montroni – Giulia Magnabosco - Elena Soragni – Cristian Torri
Irene – Marta – Silvia – Alessandro – Paolo - Rosa